INSTITUTO TECNOLÓGICO DE AERONÁUTICA



Breno Felipe Penido Morato

SUBORBITAL VEHICLE SIMULATOR FOR BRAZILIAN TERRITORY MONITORING

Final Paper 2025

Course of Aerospace Engineering

Breno Felipe Penido Morato

SUBORBITAL VEHICLE SIMULATOR FOR BRAZILIAN TERRITORY MONITORING

Advisor

Cap Av. Cap Av. Lucas Oliveira Barbacovi (ITA)

Co-advisor

Prof. Dr. Christopher Shneider Cerqueira (OVNI)

AEROSPACE ENGINEERING

São José dos Campos Instituto Tecnológico de Aeronáutica

Cataloging-in Publication Data

Documentation and Information Division

Morato, Breno Felipe Penido Suborbital Vehicle Simulator for Brazilian Territory Monitoring / Breno Felipe Penido Morato. São José dos Campos, 2025.

Final paper (Undergraduation study) – Course of Aerospace Engineering–Instituto Tecnológico de Aeronáutica, 2025. Advisor: Cap Av. Cap Av. Lucas Oliveira Barbacovi. Co-advisor: Prof. Dr. Christopher Shneider Cerqueira.

1. Cupim. 2. Dilema. 3. Construção. I. Instituto Tecnológico de Aeronáutica. II. Title.

BIBLIOGRAPHIC REFERENCE

MORATO, Breno Felipe Penido. Suborbital Vehicle Simulator for Brazilian Territory Monitoring. 2025. 66f. Final paper (Undergraduation study) – Instituto Tecnológico de Aeronáutica, São José dos Campos.

CESSION OF RIGHTS

AUTHOR'S NAME: Breno Felipe Penido Morato PUBLICATION TITLE: Suborbital Vehicle Simulator for Brazilian Territory Monitoring. PUBLICATION KIND/YEAR: Final paper (Undergraduation study) / 2025

It is granted to Instituto Tecnológico de Aeronáutica permission to reproduce copies of this final paper and to only loan or to sell copies for academic and scientific purposes. The author reserves other publication rights and no part of this final paper can be reproduced without the authorization of the author.

Breno Felipe Penido Morato Rua H8A, Ap. 124 12.228-460 – São José dos Campos–SP

SUBORBITAL VEHICLE SIMULATOR FOR BRAZILIAN TERRITORY MONITORING

This publication was accepted like Final Work of Undergraduation S	Study
Breno Felipe Penido Morato	
Author	
Cap Av. Cap Av. Lucas Oliveira Barbacovi	
Advisor (ITA)	
Advisor	
Christopher Shneider Cerqueira (OVNI)	
Co-advisor	

Aos meus pais, amigos e colegas da melhor turma que já passou por essa instituição, por tornarem cada passo dessa caminhada incrível.

Acknowledgments

To my mother, Rose, for being the most present and loving possible mother. For all the effort in my youth and all the support in every single step of this journey.

To my father, Sid, for being such a role model for me, always there when I needed and always making the necessary sacrifices to help me stay on track.

Together, to my parents, for being to best ones and, even from a humble and simple background and through some very tough times, stood as my support in every aspect. Without you guys, not a single drop of this dream would be possible.

To my dearest old friends, Maria, MV, Artur, Guilherme, Miriam, Lauren. Even though we found so few opportunities to gather everyone at once, I always kept and will keep all of you in my heart.

To my classmates and peers, for so much union, companionship and as sources of help, knowledge, care and fun. You are the main reason all of this was so worth it.

To the great professors I've met and had the opportunity to learn from in this institute. Especially, Christopher, for accepting me in a tough moment and giving so much support, with care and patience.

A special appreciation for Prof. Morales, for being an absolutely badass and taking a great amount of time to help me solve unreasonable errors and bugs my model had in the last moments. Without you, the results and discussions section of this paper would be nonsense plots and about how it went wrong.

To the Breno of the past, for, despite so much adversities, challenges and hurdles, still persisting, wiping the tears, when needed, and believing in himself.

Resumo

Este trabalho de graduação propõe o estudo da viabilidade do emprego de um veículo suborbital reutilizável e manobrável para o monitoramento on-demand do território brasileiro, com foco na sua vasta costa. Diante dos desafios das dimensões continentais do Brasil e das limitações temporais de satélites para eventos dinâmicos, veículos suborbitais emergem como solução complementar. O estudo seleciona o veículo Dawn Mk-II Aurora e o sensor óptico Chameleon como bases para a plataforma.

A metodologia centrou-se na construção de um simulador no ambiente MATLAB/Simulink. Foi implementado um modelo de massa-ponto (point-mass) bidimensional, com a lógica de voo estruturada como uma máquina de estados finitos (decolagem, subida motorizada e voo livre). A dinâmica de voo utilizou blocos do Aerospace Blockset e um controlador PID foi aplicado para gerenciar o ângulo de trajetória durante a subida.

Um estudo de caso simulou uma trajetória da costa de Natal (RN) a Vitória (ES). O simulador gerou um perfil de voo completo, atingindo um apogeu de aproximadamente 115 km e um tempo total de voo de 2596 segundos. Notavelmente, o modelo capturou dinâmicas de voo complexas, incluindo o fenômeno de "skip-glide" (quicadas) durante a reentrada atmosférica. A análise dos resultados validou a viabilidade técnica do simulador, porém revelou uma limitação crítica: o alcance horizontal obtido (aprox. 1127 km) foi insuficiente para os 1700 km desejados da rota.

Conclui-se que, para a viabilidade operacional da missão, o modelo necessita de evolução para incluir uma fase de cruzeiro motorizado no apogeu, permitindo o controle preciso do alcance. O trabalho contribui com uma ferramenta de simulação validada e estabelece os próximos passos para a integração com o laboratório ConceptIO.

Abstract

This graduation thesis proposes a feasibility study on the use of a reusable and maneuverable suborbital vehicle for on-demand monitoring of Brazilian territory, focusing on its vast coastline. Faced with the challenges of Brazil's continental dimensions and the temporal limitations of satellites for dynamic events, suborbital vehicles emerge as a complementary solution. The study selects the *Dawn Mk-II Aurora* vehicle and the *Chameleon* optical sensor as the basis for the platform.

The methodology focused on building a simulator in the *MATLAB/Simulink* environment. A two-dimensional point-mass model was implemented, with the flight logic structured as a finite-state machine (take-off, powered ascent, and free-flight). Flight dynamics utilized *Aerospace Blockset* blocks, and a PID controller was applied to manage the flight path angle during ascent.

A case study simulated a trajectory from the coast of Natal (RN) to Vitória (ES). The simulator generated a complete flight profile, reaching an apogee of approximately 115 km and a total flight time of 2596 seconds. Notably, the model captured complex flight dynamics, including the "skip-glide" phenomenon during atmospheric reentry. The analysis of the results validated the simulator's technical feasibility but revealed a critical limitation: the horizontal range obtained (approx. 1127 km) was insufficient for the desired 1700 km route.

It is concluded that for the mission's operational viability, the model must be evolved to include a powered cruise phase at apogee, allowing for precise range control. The work contributes a validated simulation tool and establishes the next steps for integration with the Conceptio laboratory.

List of Figures

FIGURE 2.1 –	Illustrative diagram of the difference between passive and active instruments (NASA, s.d.a)	21
FIGURE 2.2 –	Demonstration of the application of modeling a structure in CAE software	28
FIGURE 3.1 –	Dawn Mk-II Aurora Vehicle.(Airport Technology, 2024)	35
FIGURE 3.2 –	Photo of the Chameleon sensor	38
FIGURE 3.3 –	Point-mass model dynamics blocks from the $Aerospace\ Blockset\ toolbox$	39
FIGURE 3.4 –	Block ISA Atmosphere Model	41
FIGURE 3.5 –	Mass variation during ascent	41
FIGURE 3.6 –	Logic implemented to define when takeoff has occurred	42
FIGURE 3.7 –	Logic implemented to define when the engine is shut down	42
FIGURE 3.8 –	Block PID Controller	43
FIGURE 4.1 –	Mission Profile. In the upper images, the mission's ground track with a view of Brazil and a three-dimensional top-down view of the trajectory on the globe. Below, the two-dimensional flight profile	46
FIGURE 4.2 –	Flight profile during takeoff	48
FIGURE 4.3 –	Behavior of the aircraft's velocity throughout the flight	49
FIGURE 4.4 –	Behavior of the aircraft's velocity at takeoff	50
	Behavior of the aircraft's altitude throughout the flight as a function of time	50
FIGURE 4.6 –	Behavior of the aerodynamic forces in the aircraft throughout the flight	51
FIGURE A.1 -	-Complete block model	66

LIST OF FIGURES	X

FIGURE A.2 -	-Blocks to control the values of C_L and thrust for each phase of the	
	flight	66
FIGURE A.3 -	-Block Calculate variable mass to get the variable mass and weight	
	throughout the flight	66

List of Tables

TABLE 3.1 –	Summary of the main characteristics of the chosen vehicle (Airport	
	Technology, 2024; Dawn Aerospace, 2024)	36
TABLE 3.2 –	Summary of the main characteristics of the Chameleon sensor (Drag-	
	onfly Aerospace, 2024)	38
TABLE 3.3 –	Values used for the PID controller gains	43
TABLE 4.1 –	Input parameters for the simulation for the proposed case	45

Contents

1	INT	ΓRΟΙ	OUTION	14
	1.1	Con	ntext and Motivation	14
	1.1	1.1	The Challenge of Territorial Monitoring in Brazil	14
	1.1	1.2	Current Limitations of Satellite Remote Sensing	15
	1.2	Solu	ntion Hypothesis: Reusable and Maneuverable Suborbital Vehicles	15
	1.3	Obj	ective	16
	1.4	Stru	acture of the Text	17
2	Fu	NDA	MENTALS AND LITERATURE REVIEW	18
	2.1	Ren	note Sensors	18
	2.1	1.1	Physical principles of remote sensors	18
	2.1	1.2	Classification of remote sensing systems	20
	2.1	1.3	Types and characteristics of remote sensors	21
	2.2	Sub	orbital Vehicles	22
	2.2	2.1	Types of suborbital vehicles	23
	2.2	2.2	Applications and purposes of suborbital vehicles	23
	2.2	2.3	Characteristics and performance parameters	24
	2.2	2.4	Suborbital vehicle architecture	25
	2.3	Mo	deling and Simulation	27
	2.3	3.1	What is modeling?	27
	2.3	3.2	What is simulation?	28
	2.3	3.3	The importance of modeling and simulation in engineering	28
	2.4	Exa	mples of Applications and Scientific Publications	29

	2.5 Cha	aracteristics of the Work Context	30
	2.5.1	International Panorama of Reusable Suborbital Vehicles	30
	2.5.2	The Brazilian Aerospace Ecosystem and Technological Maturity $\ . \ . \ .$	31
3	Метно	ODOLOGY	33
	3.1 Ma	terials and Methods	33
	3.1.1	Simulation Interface	33
	3.1.2	Selection and Characterization of the Suborbital Vehicle	33
	3.1.3	Selection and Characterization of the Optical Sensor	36
	3.2 Sim	nulator Architecture and Operation	38
4	RESUL	TS AND DISCUSSIONS	44
	4.1 Pro	pposed Case Study	44
	4.2 Res	sults and Discussions	45
	4.2.1	Trajectory	45
	4.2.2	Analysis of flight profiles	48
	4.2.3	Model Limitations and Next Steps	52
5	Conci	LUSION	54
Е	BIBLIOGR.	APHY	56
A	APPENDIX	x A	60
	A.1 Sc	ript in $MATLAB$ used	60
	A.2 Blo	ock model in Simulink	66

1 Introdution

1.1 Context and Motivation

1.1.1 The Challenge of Territorial Monitoring in Brazil

Brazil, with a total area of 8,514,877 km² (Instituto Brasileiro de Geografia e Estatística (IBGE), 2024), presents continental dimensions that impose complex and multifaceted challenges regarding territorial monitoring. The management and protection of such a vast and ecologically diverse space demand cutting-edge technological solutions and innovative approaches.

Beyond its land territory, the country has an extensive coastline of 8,698 km (Secretaria do Meio Ambiente (SEMA), 2007) and the strategic "Amazônia Azul", an expanded maritime area totaling about 5.7 million km² (Marinha do Brasil, 2023). This vast oceanic area is of enormous economic and strategic importance, as approximately 95% of the national oil is extracted from it and 95% of the country's foreign trade transits through its waters (Marinha do Brasil, 2023). Safeguarding these vital resources and trade routes is a fundamental pillar for the Brazilian economy and sovereignty, and therefore, continuous and effective monitoring is crucial for national security, sustainable management of natural resources, disaster prevention and response, as well as combating illicit activities.

Earth observation by satellites is widely recognized as an indispensable tool for analyzing environmental changes and managing resources, especially considering the magnitude of the Brazilian territory. This technology simplifies and increases monitoring efficiency, being particularly relevant for a country with Brazil's biodiversity and natural resources. The need for timely actions to correct, treat, and resolve environmental problems or disasters is pressing, as a delay in response can amplify the damage and its consequences (Agência Espacial Brasileira, 2020a). The current inefficiency in monitoring, such as the lack of reliable data on illegal fishing and the proliferation of illicit activities, has direct economic and social costs, making the search for innovative solutions a national priority.

1.1.2 Current Limitations of Satellite Remote Sensing

Although remote sensing satellites are essential instruments for large-scale Earth observation, they have significant limitations, especially in terms of temporal resolution, i.e., the frequency with which they can revisit the same area. Landsat series satellites, for example, widely used for environmental monitoring, have a revisit period of 16 days. This implies that an image of a specific area can only be obtained every 16 days (Empresa Brasileira de Pesquisa Agropecuária (Embrapa), 2020), an insufficient interval to monitor dynamic and unforeseen events that evolve in a matter of hours. Even satellites with a wider imaging orbit, such as NOAA-AVHRR, which cover the Earth's surface daily, may be insufficient for the continuous detection and monitoring of rapid or localized phenomena.

Satellites are, by design, optimized for global coverage and long-term monitoring, providing a high-level view essential for climate monitoring and large environmental changes, for example. However, their fixed orbit and revisit time make them inherently less efficient for on-demand situations, i.e., localized and rapidly evolving events, such as forest fires or oil spills. This situation creates a critical operational gap in the remote sensing capability for "rapid response" to unforeseen events, which current orbital platforms cannot optimally fill and justifies the search for complementary platforms with greater flexibility and agility, capable of providing near-real-time data with greater granularity for specific areas of interest.

It is important to understand that we are talking about several different types of unforeseen events. Brazil registers more than 300,000 fire hotspots annually, with smoke clouds covering millions of km² and devastating about 15,000 km²/year of natural forests (Instituto Nacional de Pesquisas Espaciais, 2025). The 16,886 km land border with ten South American countries is a gateway for various illicit activities, including drug trafficking, arms trafficking, human trafficking, smuggling, biopiracy, and illegal exploitation. Furthermore, there are still deforestation in the Amazon and Cerrado, the growing extent of illegal fishing, piracy, water pollution, oil spills on the coast, and other state interests.

1.2 Solution Hypothesis: Reusable and Maneuverable Suborbital Vehicles

Suborbital vehicles can represent a "missing link" between satellites and aircraft. They operate in an altitude range that is too high for conventional aircraft and too low for low-orbit satellites. They are designed for scientific measurements and experiments on suborbital flights, reaching altitudes between 48 and 145 km. Their flight time is typi-

cally brief, from 5 to 20 minutes, but sufficient for specific experiments and *in situ* data collection, being ideal for regions of space that are too low for satellites (below 400 km), providing the only platforms that can perform measurements in these regions.

The operational advantages of suborbital vehicles for remote sensing are noteworthy. In terms of temporal and spatial resolution, they allow more frequent access to the space environment and control over data acquisition time, which is critical for avoiding clouds and obtaining data at multiple or specific times of the day. This *timing* capability is fundamental for capturing fleeting events. Furthermore, the maneuverability, flexibility, reusability, and cost-effectiveness of these vehicles are also major advantages for executing certain missions.

Given the above, this work is guided by the following main research question: Is it technically feasible, through computational simulation, to demonstrate that a system composed of the reusable suborbital vehicle Dawn Mk-II Aurora and the optical sensor Chameleon offers an effective and responsive solution for the *on-demand* monitoring of dynamic events in the Brazilian territory (such as oil spills or fires), overcoming the temporal revisit gaps of current observation satellites?

The foundation of the proposal is based not only on the advantages presented, but also on the fact that a project of this caliber could make use of the growing maturity that the Brazilian space industry has experienced, given projects already completed or underway, such as the VSB-30 and Avibras's TRL 6, the advances in liquid and hybrid propulsion by Edge of Space, and the 14-X by the FAB (Brazilian Air Force). Furthermore, the advancements still needed to execute the project will further increase Brazil's technological maturity in the aerospace and defense sectors (Agência Espacial Brasileira, 2022).

1.3 Objective

Therefore, this work has the following main objectives:

- Study models of suborbital vehicles and optical sensors. In particular, their characteristics, capabilities, specifications, and differences between the main models on the market;
- Model and simulate a suborbital vehicle defined after the previous study, along with its optical sensor, extracting data such as trajectory, flight time, and sensor performance;
- Integrate the built simulator into the Conceptio laboratory's simulation environment.

1.4 Structure of the Text

To answer the research question and achieve the proposed objectives, this graduation thesis is structured as follows:

- Chapter 1 Introduction: Presents the context of territorial monitoring in Brazil, the limitations of current solutions, and the hypothesis of using suborbital vehicles, culminating in the objectives and the research question.
- Chapter 2 Fundamentals and Literature Review: Provides the necessary theoretical background, addressing the principles of remote sensors, the characteristics, types, and architectures of suborbital vehicles, and the fundamentals of modeling and simulation applied to engineering.
- Chapter 3 Methodology: Describes the materials used, justifying the choice of the MATLAB/Simulink environment as the simulation interface. It presents the selection process and detailed characterization of the simulator's central components: the Dawn Mk-II Aurora suborbital vehicle and the Chameleon optical sensor. It shows a generic operation of the proposed solution.
- Chapter 4 Results and Discussions: Presents the case study in a defined monitoring scenario and discusses the results obtained. It analyzes whether the work's objectives were achieved.
- Chapter 5 Conclusion: Presents the synthesis of the results obtained, answers the research question about the platform's feasibility, discusses the integration with the Conceptio laboratory, and suggests future work.

2 Fundamentals and Literature Review

2.1 Remote Sensors

Remote sensing represents a fundamental discipline in applied sciences, allowing the acquisition of information about the Earth's surface and other celestial bodies without the need for direct physical contact. This capability is made possible by specialized instruments, known as remote sensors, which can be installed on various platforms, such as satellites, spacecraft, or aircraft. The essence of this technology lies in the detection and recording of electromagnetic energy that is reflected or emitted by the objects of interest. The primary objective is to transform the raw data collected by these sensors into thematic images or structured information, which serve as a basis for in-depth analyses and strategic decision-making.

This remote approach allows for a comprehensive and repetitive view of vast areas, overcoming the limitations of traditional surveying methods. The raw data, initially composed of digital values, undergoes classification processes that convert it into simpler and more understandable thematic categories, such as urban areas, water bodies, or different types of vegetation, represented by a clear legend. The utility of remote sensing is multifaceted. It allows for the synoptic observation of large extensions of the Earth's surface in a single image, which is crucial for large-scale environmental monitoring, natural resource planning, disaster management, and countless other applications in geosciences and applied sciences. For example, it is employed to map land use and land cover, monitor deforestation, assist in weather forecasting, and assess water resource availability. The ability to collect information repetitively at different scales – spatial, temporal, and spectral – gives remote sensing invaluable worth for the understanding and management of mission data.

2.1.1 Physical principles of remote sensors

The basis of remote sensing lies in the interaction of electromagnetic radiation (EMR) with objects on the Earth's surface. EMR is a form of energy that propagates as waves

through a vacuum, generated by charged particles in vibration. These waves have different wavelengths and frequencies, which together make up the electromagnetic spectrum (EM). The EM spectrum ranges from long-wavelength radio waves to very short-wavelength gamma rays, including microwaves, infrared (IR), visible light, ultraviolet (UV), and X-rays.

It is important to note that the human eye is sensitive to only a small portion of this spectrum, visible light, which ranges from 400 nm to 700 nm. The main source of natural energy for optical remote sensing is the Sun; when interacting with the Earth's surface, its energy can be reflected, absorbed, or transmitted by objects, in different proportions depending on the object. This variation is fundamental for remote sensing, as each object possesses a unique "spectral signature." A spectral signature is a curve that illustrates how an object's reflectance changes as a function of wavelength. For example, a green leaf reflects little energy in the visible band (due to absorption by chlorophyll for photosynthesis) and, consequently, appears dark in this range. However, it reflects high energy in the near-infrared band (due to internal cellular structure), appearing bright in this band. Remote sensors are designed to capture this reflected or emitted energy at different wavelengths, allowing for the identification and differentiation of objects based on their distinct spectral signatures.

Optical remote sensing concentrates on specific portions of the electromagnetic spectrum, primarily in the visible, near-infrared (NIR), and short-wave infrared (SWIR) bands. Each of these bands has distinct characteristics and applications that are crucial for extracting information about the Earth's surface. Visible light is the portion of the spectrum that the human eye can detect, encompassing the colors blue (400-500 nm), green (500-600 nm), and red (600-700 nm). Optical sensors capture data in these bands to create "true-color" images, which replicate human visual perception of the Earth. Additionally, the Deep Blue band (400-450 nm), which is more recent, is particularly useful for penetrating the water column, allowing for bathymetry (depth) determination and water quality assessment, overcoming light absorption and scattering by water in other bands. Near-infrared (NIR), which ranges from 0.7 to 1.0 μ m, is a range of extreme importance for vegetation studies. Healthy plants exhibit high reflectance in this band due to their cellular structure, while chlorophyll absorbs visible light for photosynthesis. This characteristic allows for the assessment of vegetation vigor and the detection of water stress or diseases. The Red Edge band (700-750 nm), located at the transition between red and near-infrared, is notably sensitive to vegetation health and vigor, making it a valuable tool for agricultural and environmental monitoring. Short-wave infrared (SWIR), covering 1 to 1.7 μ m, is useful for differentiating vegetation types, assessing soil moisture content, and identifying minerals (Kevin Enright (UP42), 2022).

The ability to capture data in multiple spectral bands, known as spectral resolution,

is a determining factor for the quantity and quality of information that can be extracted. The interconnection between the spectral signatures of targets and the spectral resolution of sensors is fundamental for the applicability of remote sensing. A sensor's spectral resolution, which defines the width and number of these bands, determines the precision with which this fingerprint can be registered. Multispectral sensors, with a few broad bands, provide a general overview, while hyperspectral sensors, with hundreds of narrow bands, capture a much more detailed "fingerprint" (NASA, s.d.a). This ability to discern finer and more numerous wavelengths allows for a much more precise discrimination between different types of materials or conditions. For example, while a multispectral sensor might map a forest area generally, a hyperspectral sensor might be able to distinguish individual tree species within that same forest. Thus, advances in spectral resolution, such as the transition to hyperspectral systems, are not merely technical improvements; they are crucial enablers that expand the frontiers of remote sensing, enabling new and more precise applications that were previously unfeasible.

2.1.2 Classification of remote sensing systems

Remote sensing systems are categorized according to the energy source they use to collect data, a fundamental distinction that defines their capabilities and operational limitations. This classification divides them into two main categories: passive sensors and active sensors.

Passive sensors are those that detect natural electromagnetic radiation reflected or emitted by the Earth's surface. They do not possess their own energy source; instead, they depend on external sources, such as reflected sunlight (for the visible and near-infrared range) or thermal energy emitted by the objects themselves (for thermal infrared) (NASA, s.d.a). Examples of passive sensors include photographic systems, radiometers, and spectroradiometers, as well as most Earth observation satellites, such as Landsat, SPOT, CBERS, and Sentinel-2 (Copernicus, s.d.). These sensors operate mainly in the visible, infrared, and thermal infrared portions of the spectrum.

Active sensors, on the other hand, are characterized by producing their own electromagnetic radiation. This energy is emitted toward the target, interacts with it (being reflected or scattered), and is then captured back by the sensor (NASA, s.d.a). The main advantage of active systems is their independence from solar illumination conditions, which allows them to operate both day and night. Notable examples of active sensors include radars, such as RADARSAT and Sentinel-1 (NASA, s.d.b), which operate in the microwave range, and lasers, such as those used in LiDAR (Light Detection and Ranging) systems and altimeters (NASA, s.d.a).

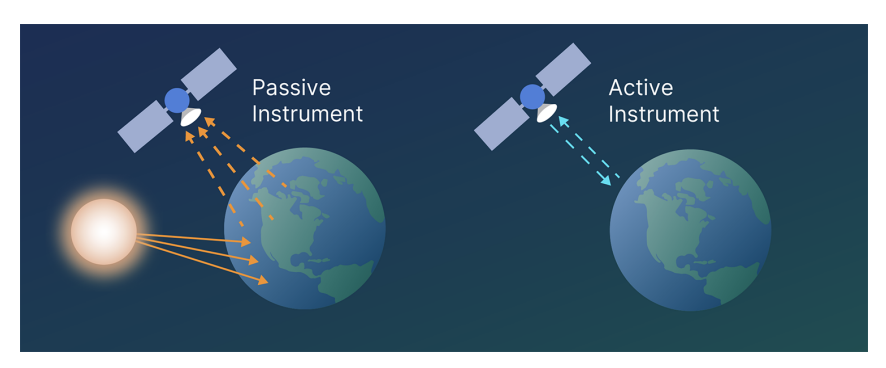


FIGURE 2.1 – Illustrative diagram of the difference between passive and active instruments (NASA, s.d.a).

2.1.3 Types and characteristics of remote sensors

The essential components of an optical sensor include (Carlos Alberto Steffen, s.d.):

- Lenses, Mirrors, and Prisms: These optical elements are responsible for focusing light and, in many cases, separating it into different spectral bands before it reaches the detectors.
- CCD (Charge-Coupled Device) Chips: At the heart of modern optical sensors, CCD chips are electronic devices composed of thousands of small radiation-sensitive cells, called detectors, organized in a matrix of rows and columns. When light is projected onto the chip, each detector is activated, generating a small electrical charge proportional to the intensity of the light received.
- Electronic System: This system is tasked with quickly reading the electrical charge value of each detector, converting it into a digital value (known as digital level or digital count value DN), and storing it in a computer file.
- **Pixel:** In the resulting digital image, each cell in the matrix corresponds to a detector on the CCD chip and is called a pixel (picture cell). The shade or brightness of each pixel is directly proportional to the digital level registered in the corresponding cell of the CCD chip.

The operation of an optical sensor involves projecting the scene's light onto the CCD chip. The generated electrical charges are then read and stored digitally. For the creation of color images, light is frequently separated into its primary components (blue, green, and red) by means of filters and prisms, and each component is projected onto a specific CCD chip (Carlos Alberto Steffen, s.d.).

Furthermore, optical sensors can be of a few main types (Carlos Alberto Steffen, s.d.):

• **Digital cameras:** Use CCD chips to capture images with greater flexibility and a wider range of applications.

- Non-conventional cameras: These are digital cameras enhanced to include bands beyond the visible spectrum, such as infrared. This capability is crucial for vegetation studies, for example, where reflectance in the near-infrared reveals information about plant health that is not visible to the human eye.
- Orbital imagers: Highly sophisticated remote sensing systems installed on artificial satellites. These platforms offer an efficient and cost-effective solution for obtaining repetitive images of large extensions of the Earth's surface over long periods. Their operation is analogous to that of an adapted digital camera, but with the capacity to generate images in multiple bands simultaneously.

Finally, without much further depth, it is relevant to cite that optical sensors also have categories based on spectral resolution, being divided into Panchromatic, Multispectral, and Hyperspectral, as simply explained previously, as well as specification categories such as spatial resolution, spectral resolution, temporal resolution, and radiometric resolution, which will be better developed during the choice of the sensor to be used for the proposed simulation.

2.2 Suborbital Vehicles

To perform an orbital flight, a spacecraft must reach what is known as orbital velocity, which is the speed necessary for an object to remain in continuous orbit around a planet, counterbalancing the gravitational force. The International Space Station (ISS), for example, which orbits Earth at about 408 km, completes an orbit every 90 minutes, traveling at approximately 27,700 km/h. Instead, a suborbital rocket flies to a certain altitude, which depends on its speed, and then returns to Earth after its engines are shut down. The trajectory of a suborbital flight is similar to a parabola, resembling the arc of a thrown ball. Although the speed of a suborbital vehicle is considerably lower than that of an orbital one (approximately 6,000 km/h to reach 200 km altitude, compared to 925 km/h for a commercial aircraft), it is still substantial.

To define what a suborbital flight is, it is important to know the Kármán line. It is widely recognized as the boundary between Earth's atmosphere and outer space, conventionally established at 100 kilometers above the Earth's surface (EBSCO, 2024). Although there are debates about its precise validity among some international entities, for the present work, it will be adopted as the limit of the atmosphere and will be used as a reference for carrying out the simulation.

2.2.1 Types of suborbital vehicles

The category of suborbital vehicles encompasses diverse platforms, each optimized for specific purposes:

- Sounding Rockets: Smaller and generally unmanned rockets, designed to carry scientific payloads to the upper atmosphere and near-space environments. They are used for measurements and scientific experiments during their suborbital flight, reaching altitudes typically ranging between 100 and 300 km, although some can reach 1,500 km. Sounding rockets are low-cost platforms, often utilizing surplus military motors, and are crucial for atmospheric studies, sampling, and remote sensing (NASA Wallops Flight Facility, 2024).
- Suborbital Reusable Launch Vehicles (SRLVs): This class of vehicles is designed for multiple flights, aiming at cost reduction and increased launch cadence. SRLVs are typically used for scientific research, technology demonstrations, and, notably, for space tourism. Prominent examples include SpaceShipOne and Blue Origin's New Shepard, which perform vertical takeoff and landing (VTOL) flights (House Committee on Science, Space, and Technology, 2012).
- Spaceplanes: Represent a fusion between rocket and conventional aircraft characteristics. These vehicles are capable of taking off and landing on runways, combining rocket performance with the operational flexibility of aircraft. The core technology of Dawn Aerospace's Aurora Spaceplane, for example, integrates extreme rocket propulsion performance with the reusability of conventional aircraft, allowing frequent and reliable access to suborbital space (Dawn Aerospace, 2024).

2.2.2 Applications and purposes of suborbital vehicles

Suborbital vehicles offer a diverse range of applications, driving advances in research, commerce, and security.

One of the most significant applications of suborbital vehicles is scientific research and technology testing. These vehicles can transport scientific experiments to space for brief periods of microgravity exposure, ranging from a few minutes to several hours, depending on the platform. This capability is invaluable for studies in various fields, such as fluid physics, biology, materials science, and combustion, where weightlessness reveals phenomena that cannot be observed on Earth. Furthermore, suborbital vehicles allow access to the upper layers of the atmosphere, enabling researchers to study these regions in ways not possible with ground-based observations or satellite measurements.

Additionally, there is also space tourism, one of the most exciting and visible prospects of suborbital vehicles. Companies like *Virgin Galactic* and *Blue Origin* are developing vehicles specifically designed to take paying passengers to the "edge of space", where they can experience a few minutes of weightlessness and observe the curvature of the Earth against the dark backdrop of space. A unique and increasingly accessible experience.

There are still other less common and largely unexplored applications, such as *Pointto-Point Transport*, which aims to use suborbital vehicles for intercontinental transport of people and cargo much faster than is done today, but will not be further developed in the present work. This is because the application to be explored here is monitoring and observation of the Earth's surface. As advantages, we can envision greater cost-effectiveness compared to satellites, high spatial and temporal resolution, with faster responses and greater flexibility of trajectories and data collection windows, essential factors for monitoring and responding to unpredictable security and defense situations. Of course, it will be important to take into account that a suborbital vehicle has more limited geographic coverage than a satellite, has a considerably short flight duration, and can more easily suffer from environmental interference, such as clouds and dust, which can hinder data collection in some conditions.

2.2.3 Characteristics and performance parameters

The typical altitude reached by suborbital vehicles is around the Kármán Line, that is, between 80 and 120 km above sea level, and their maximum speed is approximately 6,000 km/h. Their flight profile is generally divided into two characteristic parts (GOODELL; ELROD, 1995):

- Ascent: The ascent of a suborbital vehicle generally begins with a vertical or very steep engine burn, generating the necessary impulse to overcome gravity and atmospheric drag. After main engine cut-off (MECO), the vehicle enters a coasting or free-fall phase, where propulsion is zero and mass is constant, and continues to rise until reaching its maximum altitude (apogee). Historical examples include the V-2 rocket, which reached 85 km, and the X-15 (WHELAN, 2013).
- Reentry: The reentry phase is critical and complex. Suborbital vehicles, upon returning to Earth, face the challenge of dissipating large amounts of kinetic energy accumulated at hypersonic speeds. Atmospheric reentry causes intense heating due to friction with the air, with temperatures that can reach thousands of degrees Celsius (NASA Glenn Research Center, 2024). For a safe landing, the spacecraft must enter the atmosphere at a precise angle and speed, within a three-dimensional "reentry corridor." If the angle is too steep, the vehicle may overheat and burn up; if it is

too shallow, it may "skip" off the atmosphere and return to space. Reentry can be ballistic (like a missile) or with aerodynamic lift (like a space shuttle), with the latter allowing greater control over the landing site and reducing deceleration loads (FAA, 2007).

Finally, reusability is a growing design principle for suborbital vehicles, aiming for significant reduction in launch costs and increased flight frequency. A reusable launch vehicle has parts that can be recovered and reused, such as rocket stages, fairings, boosters, or engines. Recovery methods include (SARIGUL-KLIJN; SARIGUL-KLIJN, 2003):

- Vertical Landing (VTOL) with Retropropulsion: Where the vehicle decelerates and lands vertically using its own engines, like *Blue Origin*'s *New Shepard* (Wikipedia, 2024).
- Horizontal Landing (HTOL) with Wings: Similar to an aircraft, where the vehicle glides and lands on a runway, like *Virgin Galactic*'s *SpaceShipTwo* (Wikipedia, 2024).
- Parachutes and Airbags: Used to decelerate and cushion the impact upon landing, especially for capsules or recoverable stages.

It is important to note that, despite the benefits, reusability presents considerable challenges. Recovery and refurbishment costs can mitigate the benefits of not manufacturing new parts. Furthermore, reusable vehicles are subject to multiple load cycles and temperature variations, which can lead to thermal fatigue and crack propagation, requiring more durable materials and rigorous fracture control programs and post-flight inspections to ensure structural integrity.

2.2.4 Suborbital vehicle architecture

2.2.4.1 Propulsion system

The heart of any suborbital vehicle, providing the necessary impulse to reach desired altitudes and speeds. There are three main types of rocket engines used (IDU, 2024):

- Liquid Propellant Engines: Use fuels and oxidizers stored in a liquid state. They offer high performance, are controllable, and offer greater flexibility in flight trajectory and altitude control. However, they are more complex and more expensive.
- Solid Propellant Engines: Contain fuel and oxidizer mixed and molded into a single solid "grain." They are valued for simplicity, reliability, and high initial impulse. However, once ignited, they cannot be turned off or throttled, limiting mission flexibility. Most sounding rockets use solid motors.

• **Hybrid Propellant Engines:** Combine a solid fuel with a liquid oxidizer. This configuration offers a combination of safety (fuel and oxidizer stored separately), controllability (ability to turn on/off and throttle), and use of less toxic propellants compared to some liquid and solid systems. The ability to control burn time and, consequently, maximum altitude, is a significant advantage for experiments requiring precision.

2.2.4.2 Aerodynamics and Control Surfaces

The aerodynamic design of a suborbital vehicle is crucial for optimizing drag and ensuring stability during atmospheric flight phases. The fuselage shape and vehicle attitude during descent are important factors, with the sensitivity of the lift-to-drag ratio (L/D) influencing range and drag affecting maximum altitude. Design studies seek to minimize drag, with the choice of nose geometry (nosecone) being a determining factor. Aerodynamic control surfaces, such as ailerons and rudders, are used for maneuverability and attitude control at lower altitudes, where the atmosphere is dense enough to generate effective aerodynamic forces. However, at high altitudes, where the atmosphere is rarefied, these surfaces become ineffective.

2.2.4.3 Guidance, Navigation, and Control (GNC) Systems

They are responsible for determining the vehicle's trajectory, knowing its position and orientation, and executing necessary maneuvers. It comprises the following main algorithms (BOCCIA *et al.*, 2023):

- Flight Management (FM): Supervises internal status and data from all other GNC functions, defining operational modes for each component based on the flight phase and conditions.
- Guidance: Defines the reference trajectory and the control actions necessary to track it.
- Navigation: Responsible for estimating the current system state (position, velocity, and attitude). Mainly uses data from Inertial Measurement Units (IMUs) or Inertial Navigation Systems (INS).
- Control: Ensures precise tracking of reference states generated by the guidance algorithm, utilizing available GNC system actuators.

GNC flight modes are adapted to different mission phases, such as high-altitude ballistic flight, reentry burn, aerodynamic phase, and landing burn.

2.2.4.4 Structures and materials

Structural design and material selection for suborbital vehicles have the main objectives of ensuring lightness, durability, and resistance to extreme dynamic and thermal loads. The structure must be capable of withstanding significant stresses during launch and reentry, minimizing weight, which is fundamental for flight performance, while ensuring structural integrity under severe operational conditions. Reusability imposes additional requirements, such as resistance to fracture and crack propagation under fluctuating loads and chemical compatibility with contained fluids.

The most common materials for vehicles that must withstand suborbital flight conditions are metal alloys, such as aluminum-lithium (NASA, 2017), and composites, such as carbon fibers and glass fibers.

Finally, thermal protection systems (TPS) are also essential for safety during atmospheric reentry, absorbing and dissipating the intense heat generated by friction with the atmosphere. They include ablative and reusable materials, such as ceramic tiles and thermal blankets, for example (NASA Johnson Space Center, 2024).

2.3 Modeling and Simulation

Essential tools in modern engineering, modeling and simulation allow for the development and analysis of complex systems with greater efficiency, assertiveness, and lower costs.

2.3.1 What is modeling?

In the engineering context, it refers to the process of creating a simplified representation of a real-world system, process, or phenomenon. This representation, or "model", can be mathematical, computational, or physical, and aims to capture the most relevant characteristics and behaviors of the original system, ignoring details less important for the analysis in question. Modeling is fundamental for transforming continuous geometry into discrete elements, such as in mesh generation for structural analysis or volume generation for fluid dynamics, allowing the application of numerical solutions for differential equations.

2.3.2 What is simulation?

Simulating is using a model to mimic the behavior of a system over time, allowing the observation of how it reacts to different conditions or inputs. It is a technique that allows testing scenarios, optimizing designs, and predicting results without the need to build expensive and time-consuming physical prototypes. Through simulation, it is possible to estimate quantities such as mechanical stress, deformation, natural vibration frequencies, heat transfer, and electromagnetic phenomena.

2.3.3 The importance of modeling and simulation in engineering

It is difficult to estimate the boost in innovation and competitiveness that modeling and simulation generate in engineering. Their applications extend from manufacturing engineering to cyber defense, allowing engineers and researchers to face complex challenges efficiently and economically. The possibility of performing virtual tests that would be prohibitively expensive or time-consuming in the physical world, such as crash tests or flow analyses in wind tunnels, is one of the technology's main contributions, but it comes added with other major advantages. For the same reasons, modeling and simulation also optimize designs (since they allow calculations and fine adjustments without the need for physical model construction and testing), allow analysis of complex phenomena, including predicting system behavior in extreme conditions or where analytical solutions are unfeasible, and mitigate risks, as they enable the identification of errors and failures even before actual production and operation (SAHINOGLU, 2013). It is exactly in these perspectives that software like *CATIA* and *MATLAB*, from *Dassault Systèmes*, appeared, fitting into the CAD (*Computer Aided Design*) and CAE (*Computer Aided Engineering*) categories.

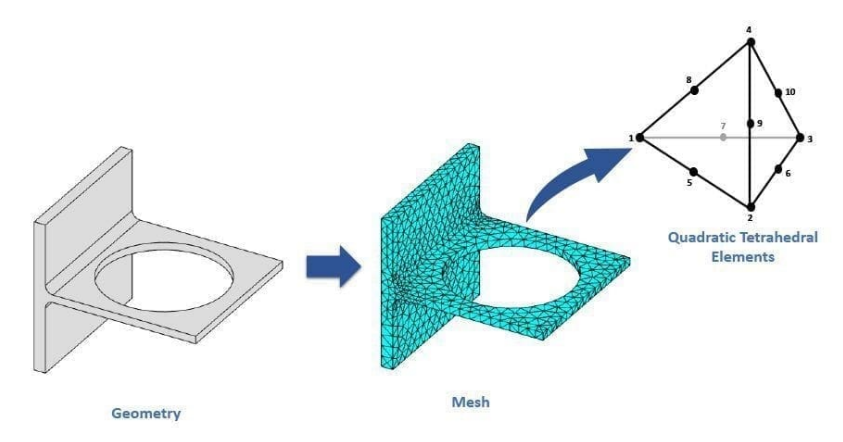


FIGURE 2.2 – Demonstration of the application of modeling a structure in CAE software.

For the present work, the simulator proves even more relevant, as, in addition to

allowing the study and optimization of the proposed vehicle, as well as its flight, it also allows the analysis of its interaction with the optical sensor and its capabilities for the proposed application.

2.4 Examples of Applications and Scientific Publications

The theoretical foundation on remote sensors, suborbital vehicles, and simulation methodologies establishes the conceptual bases of the present work, and simulating a suborbital vehicle for Earth observation is not a purely academic exercise, but rather a field of intense interest in the global aerospace community, driven by a clear and growing operational need.

The development of a "Simulator", as proposed in the objectives of this work, is a central and non-trivial step in the engineering of any aerospace vehicle. The technical literature demonstrates that creating a high-fidelity simulation environment is a complex challenge, with the chosen methodology, based on MATLAB/Simulink, being consistent with industry best practices for Verification and Validation (V&V) of Guidance, Navigation, and Control (GNC) systems.

GNC simulation is a central theme in research on reusable and hypersonic vehicles. Publications such as *GNC requirements of for a Long Range Hypersonic Transport System* detail the intricate interaction between aerodynamics, trajectory control, and safe flight corridors. For example, one identified control strategy for the SpaceLiner hypersonic vehicle is the use of bank angle modulation for trajectory control, maintaining the angle of attack (AoA) within rigorous limits during the hypersonic phase (HAYA *et al.*, 2012). This type of analysis directly informs the requirements and capabilities that the simulator to be developed in this work will need to contemplate.

The choice of the MATLAB/Simulink environment for this project is validated by cutting-edge research in the area. The article Physical Modeling and Simulation of Reusable Rockets for GNC Verification and Validation states that, as "GNC algorithms are typically tested in Simulink", the authors developed a high-fidelity physical modeling library (VLVLib, based on Modelica) specifically designed to be integrated into the Simulink environment (BELLI et al., 2024). This reference not only justifies the methodology adopted in this work but also points to future paths for improving model fidelity, such as including propellant sloshing dynamics or landing gear kinematics.

Additionally, trajectory optimization for reusable vehicles is a robust academic field of study. Works like *High-Fidelity Real-Time Trajectory Optimization for Reusable Launch Vehicles* explore advanced methods, such as pseudospectral ones, to generate optimal reentry trajectories in real-time, capable of compensating for large perturbations, such as

hurricane-force wind gusts (BHATT, 2006). Although the implementation of such algorithms is beyond the scope of this graduation thesis, its review demonstrates an in-depth understanding of the problem domain and avant-garde solutions.

2.5 Characteristics of the Work Context

To properly situate this project, it is essential to analyze it within the broader panorama of suborbital flight. A comparative analysis with major existing systems provides a performance and mission *benchmark*. More importantly, the connection with the capabilities and strategic objectives of the Brazilian aerospace sector demonstrates the relevance and viability of the proposal.

2.5.1 International Panorama of Reusable Suborbital Vehicles

The international market for suborbital flights is currently dominated by two main companies, focusing on space tourism and scientific research. The analysis of their systems offers a valuable reference for performance, mission profile, and payload capacity, highlighting the unique characteristics of the vehicle proposed in this work.

- Virgin Galactic SpaceShipTwo: a rocket-powered spaceplane launched from the air, designed to carry six passengers and two pilots. The vehicle is released at an altitude of approximately 15 km, ignites its hybrid rocket motor to reach an apogee of approximately 110 km, and then glides back for a conventional runway landing (CARR, 2011).
- Blue Origin New Shepard: a fully autonomous system composed of a capsule and a booster rocket, capable of vertical takeoff and landing (VTOL). The vehicle transports passengers or payloads beyond the Kármán Line (100 km), providing a few minutes of microgravity before the capsule returns under parachutes and the booster performs a powered vertical landing (Blue Origin, 2024).

In comparison, the Dawn Mk-II Aurora distinguishes itself by being an unmanned vehicle, smaller in size, and designed for rapid reusability with operations analogous to those of an aircraft, utilizing conventional runways. This positions it in a different market segment, prioritizing operational flexibility, agility, and cost-effectiveness over the passenger experience.

The diversity of architectures in the international market reflects a fundamental tradeoff between operational simplicity and performance. Virgin Galactic's air launch system avoids the spacecraft needing to carry propellant for the initial climb to 15 km but requires a specialized, large carrier aircraft, adding logistical complexity. Blue Origin's VTOL system is architecturally simpler in terms of the number of vehicles but requires extremely complex GNC for powered landing and dedicated ground infrastructure. Dawn Aerospace's approach, with a fully integrated HTOL (Horizontal Take-Off and Landing) system, represents a third, potentially more agile way. This concept seeks to combine the flexibility of an aircraft with the performance of a rocket, drastically reducing the need for ground infrastructure and preparation time between flights.

2.5.2 The Brazilian Aerospace Ecosystem and Technological Maturity

The proposal to develop a sovereign suborbital vehicle for monitoring does not represent a leap in the dark for Brazil, but rather a logical and strategic evolution, built upon a foundation of proven successes and ambitious projects underway. The national aerospace ecosystem has reached a Technology Readiness Level (TRL) that makes this effort not only plausible but necessary for the country's strategic interests.

The main operational foundation is the VSB-30, the most successful sounding rocket of the Brazilian Space Program. Developed by IAE/DCTA, this two-stage solid propellant vehicle has accumulated over 30 successful launches from various bases around the world, demonstrating Brazil's consolidated capacity to launch 400 kg payloads to altitudes of 270 km (Agência Espacial Brasileira, 2020b).

At the forefront of Brazilian aerospace ambition is Project 14-X, a demonstrator of a hypersonic vehicle propelled by a *scramjet* engine. The first flight test, carried out in "Operation Cruzeiro" in December 2021, was a historic milestone: launched aboard a VSB-30 rocket, the 14-X reached a speed of Mach 6 at 30 km altitude and a suborbital apogee of 160 km. Although hypersonic dynamics are not the scope of the present work, the 14-X project proves national mastery of critical technologies such as high-speed aerodynamics, air-breathing propulsion, and advanced materials, all directly applicable to a real project of a reusable spaceplane.

Analyzing the trajectory of these projects, a clear path of technological evolution emerges within the Brazilian space program: from the VSB-30, passing through the 14-X, to the concept of a reusable monitoring vehicle proposed in this work. The VSB-30 represents the mastery of ballistic suborbital flight and solid propulsion. The 14-X project uses this launch capability as a platform to explore the much more complex domain of atmospheric hypersonic flight, which involves challenges of control, materials, and thermal management, the same challenges faced during the reentry of a reusable vehicle. The use of the VSB-30 as a booster for the 14-X is the most explicit evidence of this technological connection. The project proposed in this thesis, therefore, positions itself at the confluence

of these efforts: it combines the mission of a sounding rocket with the reusability and maneuverability of a glider.

3 Methodology

3.1 Materials and Methods

3.1.1 Simulation Interface

For the present work, the *MATLAB/Simulink* environment was selected as the main interface for the development of the suborbital vehicle and optical sensor simulator. This is because it is a tool widely adopted in aerospace engineering, both in academia and industry, due to its versatility and processing power.

Firstly, Simulink is recognized for its excellence in modeling complex dynamic systems. Its block-based graphical interface allows for the intuitive construction of models representing propulsion, aerodynamics, control, and sensor subsystems in a modular fashion. This feature facilitates the representation of aerial and space vehicles, allowing the focus to be on system dynamics rather than low-level coding of each component.

Secondly, the synergy between Simulink and MATLAB is a significant differentiator. MATLAB offers a vast set of function libraries for data analysis, optimization, signal processing, and visualization. This integration is essential for post-processing simulation results, implementing control and navigation algorithms, and analyzing the performance of the vehicle-sensor system. The availability of specific toolboxes, such as the Aerospace Toolbox, Control System Toolbox, and Image Processing Toolbox, provides pre-built resources that accelerate development and ensure the robustness and accuracy of the models.

Additionally, the tool will optimize project resources and time, given familiarity with it, as well as facilitate the integration of the developed simulator with the Conceptio Laboratory's simulation environment.

3.1.2 Selection and Characterization of the Suborbital Vehicle

A market survey was conducted in search of models and prototypes that meet the criteria and hypotheses of the proposed project. In particular, the following criteria were

significantly taken into consideration:

- Reusability;
- Maneuverability;
- Market existence (or prototype in an advanced stage of development);
- Payload capacity, for transporting the optical sensor.

Thus, after the market survey, among several relevant models present in the market, such as sounding rockets (e.g., Copenhagen Suborbitals Spica) and reusable launch vehicles (e.g., SpaceX Falcon 9), it was possible to arrive at some main candidates:

• Virgin Galactic SpaceShipTwo (VSS Unity):

- Manned suborbital spaceplane, launched from a mother aircraft (White Knight Two);
- It is reusable, designed for multiple commercial and research flights;
- Being a piloted spaceplane, it is maneuverable and performs a gliding return flight for a conventional runway landing;
- It is air-launched (approximately 15.2 km), with rocket motor ignition to reach an apogee of about 80-90 km and speeds from Mach 2.9 to 3.2.
- Designed to carry up to 6 people.

• Dawn Mk-II Aurora (Dawn Aerospace):

- Unmanned rocket-powered suborbital spaceplane, designed to take off and land on conventional runways;
- Designed for rapid reusability, with the capacity to perform multiple flights per day;
- Takes off and lands like a conventional aircraft, allowing for customizable trajectories and controlled landing;
- Reaches altitudes above 100 km and speeds exceeding Mach 3.5. Has already demonstrated supersonic flights (Mach 1.1) and altitudes of 25 km;
- Has a dedicated payload bay of up to 10 kg, with dimensions of 30cm x 10cm x 10cm, and an optical window.

• Andromach Suborbital Spaceplane:

- Suborbital spaceplane, with a reusable design;

- Takes off from a conventional runway using turbojet engines, activates the rocket engine over the ocean, reaches space, and returns gliding for a runway landing;
- Reaches apogee of 100-200 km, with a maximum speed of Mach 5 and maximum acceleration of 4g;
- Payload capacity of up to 30 kg.

The analysis of the candidates reveals some clear distinctions. Firstly, the Virgin Galactic SpaceShipTwo does meet the project requirements, but it is a people transport vehicle, focused, therefore, on space tourism, *point-to-point* travel, or, at most, conducting specific microgravity experiments.

The Andromach Suborbital Spaceplane is a project outside the scope of this work: hypersonic and with a dual propulsion system (turbojets and rocket), factors that would add unnecessary complications to the project, such as analysis of resistance and behavior of the optical sensor in the hypersonic regime and a propulsion system being altered mid-flight.

Therefore, the choice made was the Dawn Mk-II Aurora from Dawn Aerospace as the most suitable model for carrying out the project.



FIGURE 3.1 – Dawn Mk-II Aurora Vehicle. (Airport Technology, 2024)

Characteristic	Orbital Satellite
Length	4.8 m
Take-off mass	280 kg
Empty mass	$75~\mathrm{kg}$
Propulsion	HTP / Kerosene
Maximum altitude	$\sim 100 \text{ km}$
Maximum speed	Mach 3.5
Horizontal range	Between 50 km and 80 km
Payload capacity	10 kg, with $30 x 10 x 10 cm$

TABLE 3.1 – Summary of the main characteristics of the chosen vehicle (Airport Technology, 2024; Dawn Aerospace, 2024).

3.1.3 Selection and Characterization of the Optical Sensor

Reusability

Analogously to what was done with the suborbital vehicle, a market survey was conducted in search of optical sensors that meet the project's needs. The main criteria used were:

Multiple flights per day

- Optical type;
- High spatial resolution (GSD Ground Sample Distance);
- Market existence (or prototype);
- Weight within the chosen vehicle's capacity.

The survey identified the following most relevant models on the market:

- **Specim AFX10:** (Specim, 2024)
 - Type: Compact hyperspectral camera;
 - Spectral Range: VNIR (400 1000 nm);
 - Weight: 2.1 kg (without gimbal);
 - Power Consumption: 17 W;
 - Resolution (Pixels): 512 x 1024;
 - Spectral Bands: 224 bands;
 - GSD: 3.5 cm at 50 m altitude, 7.0 cm at 100 m, 10.5 cm at 150 m;

- Applications: Vegetation classification, water quality analysis, wetland monitoring, wildlife population studies.

• Chameleon (Dragonfly Aerospace): (Dragonfly Aerospace, 2024)

- Type: Compact high-resolution multispectral cameras;
- Spectral Range: 150 bands, in the IR spectrum;
- Weight: 1.6 kg;
- Power Consumption: 10 W during imaging;
- Spectral bands: 11 x MS;
- GSD: 10 m at 500 km altitude;
- Applications: Earth observation, including agricultural yield planning, soil condition assessment, and emergency response.

• Ximea xiSpec: (Ximea, 2024)

- Type: Compact hyperspectral camera;
- Extremely compact (32g);
- Low consumption (< 1.5W);
- Spectral range between 460-960 nm and 15-150 bands;
- Resolution: 2.2 MPix;
- Ideal for UAVs and remote sensing.

• Landsat 9: (GIM International, 2024)

- Type: Satellite panchromatic/multispectral sensors;
- 11 spectral bands, with spatial resolutions of 15 m (panchromatic), 30 m (most reflective bands), and 100 m (thermal bands);
- Application: Excellent for large-scale Earth observation. Designed for orbital platforms.

The requirement for "monitoring Brazilian territory" and the need to "track an event" for which the temporal resolution of satellites may be insufficient imply a demand for high spatial resolution and detailed spectral information. This strongly favors the use of compact hyperspectral sensors, which can operate on suborbital platforms and offer GSDs significantly superior to orbital sensors, in addition to providing rich data for material identification.

Therefore, based on the analysis, the Chameleon model from Dragonfly Aerospace was chosen as the optical sensor for carrying out the project.



FIGURE 3.2 – Photo of the Chameleon sensor.

TABLE 3.2 - Summary of the main characteristics of the Chameleon sensor (Dragonfly Aerospace, 2024).

Characteristic	Orbital Satellite
Spectral range	Infrared
Weight	$1.6~\mathrm{kg}$
Dimensions	$10~\mathrm{cm}~\mathrm{x}~10~\mathrm{cm}~\mathrm{x}~21.5~\mathrm{cm}$
Power consumption	10 W (during imaging)
Number of spectral bands	$11 \times MS$
Data format	10-bit or 12-bit
Swath width (Swath)	39 km
GSD	$10~\mathrm{m}$ at $500~\mathrm{km}$ altitude

3.2 Simulator Architecture and Operation

The methodology for constructing the simulator was based on a simplified approach, using a *point-mass* model to represent the vehicle's dynamics in a two-dimensional plane.

The core of the simulation logic was implemented as a finite-state machine. This architecture segments the flight into distinct phases, each with different parameters and transition conditions. The transition between states is controlled using *Switch* blocks in *Simulink*, which activate or deactivate variables or change their values. The flight dynamics itself was modeled using the fourth-order point-mass blocks available in the *Aerospace Blockset toolbox*, which integrate the equations of motion to calculate the vehicle's position and velocity over time.

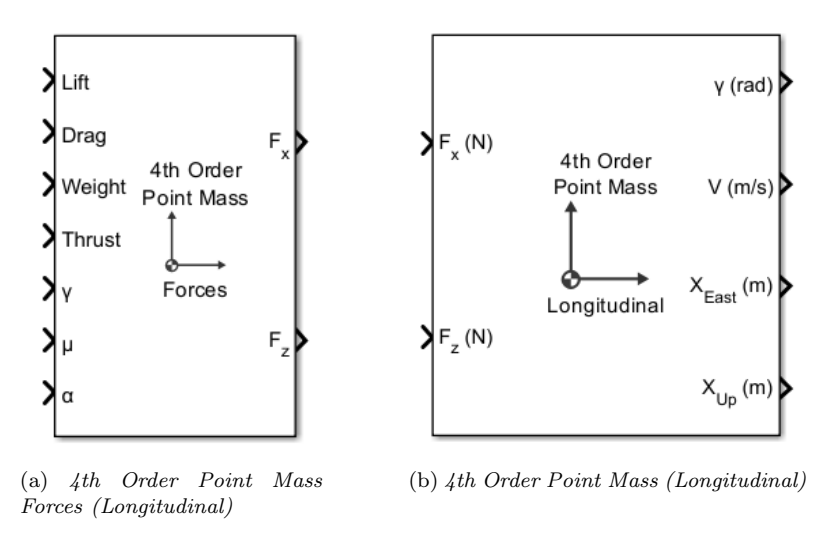


FIGURE 3.3 – Point-mass model dynamics blocks from the Aerospace Blockset toolbox

Block 3.3a follows a simple force decomposition algorithm:

$$\begin{cases} F_z = (L + T \sin \alpha) \cos \mu - W \cos \gamma \\ F_x = T \cos \alpha - D - W \sin \gamma \end{cases}$$
(3.1)

Where,

L = Lift force

D = Drag force

W = Weight

T =Engine thrust

 $\gamma = \text{Flight path angle}$

 $\mu = \text{Bank angle}$

 $\alpha = \text{Angle of attack}$

Block 3.3b follows a simplified flight mechanics algorithm (MIELE, 1962):

$$\begin{cases} F_x = m\dot{V} \\ F_z = mV\dot{\gamma} \\ \dot{X}_{east} = V\cos\gamma \\ \dot{X}_{up} = V\sin\gamma \end{cases}$$
(3.2)

Where,

V = Resultant velocity

 $\dot{X}_{east} = \text{Horizontal distance}$

 $\dot{X}_{up} = \text{Altitude}$

To build the model, it is necessary to provide the 4th Order Point Mass Forces block (3.3a) with its proper inputs.

First, for lift, the relation (ANDERSON; EBERHARDT, 2021) was used:

$$L = \frac{1}{2}\rho V^2 C_L A \tag{3.3}$$

Where,

 $\rho = Air density$

 $C_L = \text{Lift coefficient}$

A = Wing area

The C_L is considered constant in each phase and has one value during takeoff, another during the powered ascent, and is zero from the moment the engine is shut down.

Analogously, for drag:

$$D = \frac{1}{2}\rho V^2 C_D A \tag{3.4}$$

However, here, unlike the lift case where the coefficient is estimated and provided as a parameter for each flight phase, C_D is obtained from the simplified induced drag relation, known as the parabolic drag polar (ANDERSON; EBERHARDT, 2021):

$$C_D = C_{D_0} + k_{drag} C_L^2 (3.5)$$

Where,

 C_{D_0} = Parasite drag coefficient (at zero AoA)

 $k_{drag} =$ Induced drag factor

It is important to explain how air density is being obtained. For small altitude variations, it also varies little. However, in this case, we are simulating a flight that ranges from sea level - where density is maximum - to near the Kármán line - where it is prac-

tically zero. For the present work, the International Standard Atmosphere (ISA) model was used, which was done using a block also from the *Aerospace Blockset toolbox*.

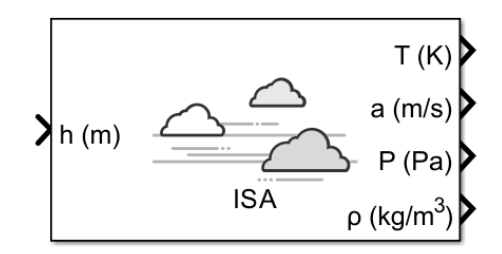


FIGURE 3.4 - Block ISA Atmosphere Model

The model employed by the block in Figure 3.4 follows a logic of dividing the atmosphere into layers with different temperature lapse rates, considering pressure varying exponentially, and obtaining density at each point from these parameters (INTERNATIONAL ORGANIZATION FOR STANDARDIZATION, 1975).

For weight, according to Table 3.1, it varies from 280 kg at takeoff to 75 kg when empty of fuel. For simplicity, this variation will be considered linear between the start of takeoff and the end of the burn, just before the start of free flight.

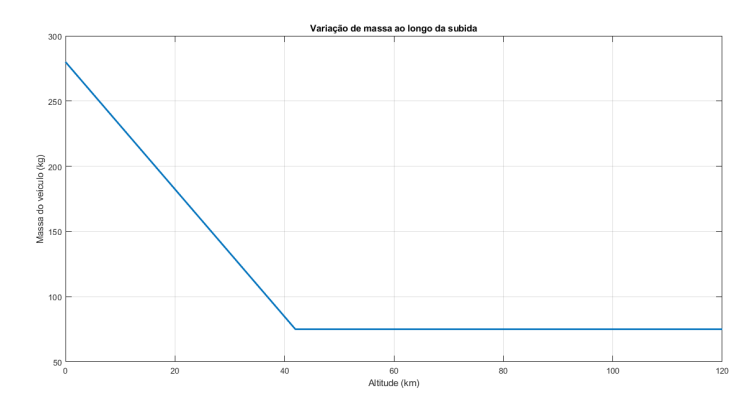


FIGURE 3.5 – Mass variation during ascent.

For thrust, a simple control was built using Switch blocks. Thrust, like C_L , is considered constant in each phase and has one value during takeoff, another during powered ascent, and is zero from the moment the engine is shut down.

The bank angle μ is constant zero throughout the flight, as the present work simplifies it by limiting it to the vertical X-Z plane.

For the angle of attack (AoA) α , the standard lift curve in the linear region (for low angles of attack) was used (ANDERSON; EBERHARDT, 2021):

$$C_L = C_{L_0} + C_{L_\alpha} \alpha \tag{3.6}$$

Where,

 $C_{L_0} = \text{Lift coefficient at zero AoA}$

 $C_{L_{\alpha}}$ = Lift curve slope (rate of change of C_L with α)

Finally, the flight path angle γ is an output of the 4th Order Point Mass block and, therefore, also used as an input here, feeding back into the system.

The conditionals for the *Switch* blocks are obtained from relational blocks (*Relational Operator*). For example, for takeoff, the block compares lift with weight. The result is zero while lift has not yet overcome weight, and 1 from the moment it does.

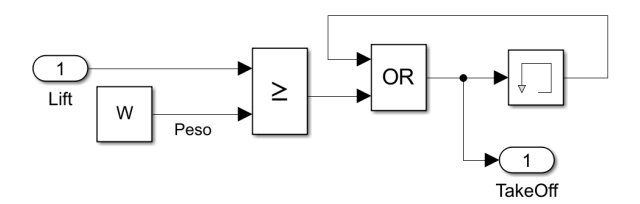


FIGURE 3.6 – Logic implemented to define when takeoff has occurred.

One detail worth noting is the use of the Logical Operator and Memory blocks to ensure that, from the moment takeoff has occurred, even if the L > W condition is not met at some point in flight, the value of the TakeOff variable does not revert to zero. Thus, the model no longer returns to the takeoff state once it is complete, and the TakeOff variable can be used as a conditional in the Switch blocks that control thrust and C_L .

An analogous logic was implemented to check the free-flight condition, but now comparing the altitude with h_{MECO} (main engine cut-off, altitude at which the engine is shut down).

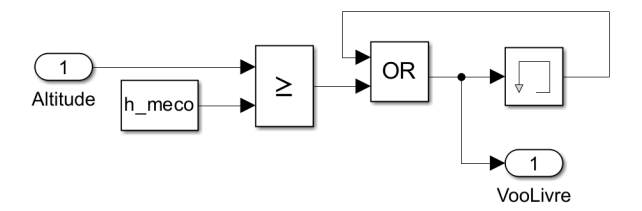


FIGURE 3.7 – Logic implemented to define when the engine is shut down.

PID Controller

To avoid anomalous results, a different methodology was implemented in the powered ascent phase of the vehicle. The pillar of this methodology is the PID (Proportional-Integral-Derivative) controller. The PID controller's strategy is to generate a control

signal, u(t), which is the weighted sum of three distinct terms, all based on the error signal e(t). According to canonical works in control engineering, the "ideal" or "standard" form of the PID controller in continuous time is described by the following equation:

$$u(t) = K_p e(t) + K_i \int_0^t e(t)d\tau + K_d \frac{d}{dt}e(t)$$
 (3.7)

Where,

e(t) = r(t) - y(t) is the error signal at time t.

u(t) is the controller output (control signal) at time t.

 K_p is the Proportional gain.

 K_i is the Integral gain.

 K_d is the Derivative gain.

The "tuning" process of the controller consists of finding the optimal values for K_p , K_i , and K_d that make the closed-loop system respond in the desired manner (e.g., fast, stable, and precise). For the present work, the *PID Controller* block from *Simulink* was used.

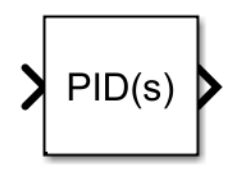


FIGURE 3.8 – Block PID Controller

In it, the input is the error between the desired flight path angle (γ) and the current one $(\gamma_{subida} - \gamma)$, and the output is the ascent C_L (with engine on). Note that the flight path angle at any moment in the simulation is one of the outputs of the 4th Order Point Mass block. By adjusting the block's gains, it was possible to obtain a set of values that allow tracking.

Value
0.1
1
0

TABLE 3.3 – Values used for the PID controller gains.

4 Results and Discussions

4.1 Proposed Case Study

The case study for this work consists of a suborbital flight departing from a hypothetical launch base near Natal, Rio Grande do Norte, and landing at a hypothetical base near Vitória, Espírito Santo. The choice of this route is strategic, as it allows for continuous monitoring of an extensive stretch of the Brazilian coast, an area of vital economic and security importance, as discussed in the motivation for this work.

Thus, the proposed mission is to generate a trajectory that connects the two points, simulating the flight of the Dawn Mk-II Aurora vehicle in a vertical plane, and to evaluate the continuous terrain monitoring capability under the flight path, using the parameters of the Chameleon optical sensor. In particular, some of the main mission constraints are:

- Maximum altitude: the vehicle must reach an altitude close to 100 km at its highest point on the trajectory.
- Range: the vehicle must have a horizontal range (between takeoff and landing) of approximately 1700 km, which is the approximate straight-line distance between the proposed bases.
- Maximum velocity: as the developed model is a simplification, for its result not to deviate excessively from reality, it is desirable that the vehicle never enters the hypersonic region (approximately Mach 5 or 1700 m/s), where the dynamics and motion equations begin to show significant differences from those used here.

Table 4.1 presents the parameters entered for this case study.

Parameter	Value	
Take-off mass	280 kg	
Empty mass	75 kg	
Estimated wing area	$7.5~\mathrm{m}^2$	
Minimum lift coefficient (C_{L_0})	0.1	
Lift curve slope $(C_{L_{\alpha}})$	2.8	
Minimum drag coefficient (C_{D_0})	0.02	
Induced drag factor (k_{drag})	0.2	
Take-off C_L	0.2	
Ascent C_L (engine on)	variable	
Free-flight C_L	0.13	
Take-off thrust	2000 N	
Ascent thrust (engine on)	6000 N	
Free-flight thrust (engine off)	0 N	
Main engine cut-off altitude (h_{MECO})	42 km	

TABLE 4.1 – Input parameters for the simulation for the proposed case.

An important practical observation is that the initial parameters for flight path angle, altitude, and horizontal position are zero, provided to the 4th Order Point Mass block, but the initial velocity provided is 1 m/s. This is due to a limitation of the physical model used by the block which prevents the velocity from being zero at any time during the simulation, evident from Equation 3.2.

4.2 Results and Discussions

The execution of the simulation, with the presented parameters, in the MATLAB/Simulink environment generated a dataset that describes the vehicle's behavior throughout the entire mission. The main results are presented and analyzed below.

4.2.1 Trajectory

The primary result of the simulator is the complete trajectory of the vehicle, which can be visualized graphically. Figure 4.1 presents the obtained path, bidimensionally and tridimensionally, connecting the launch and landing bases.

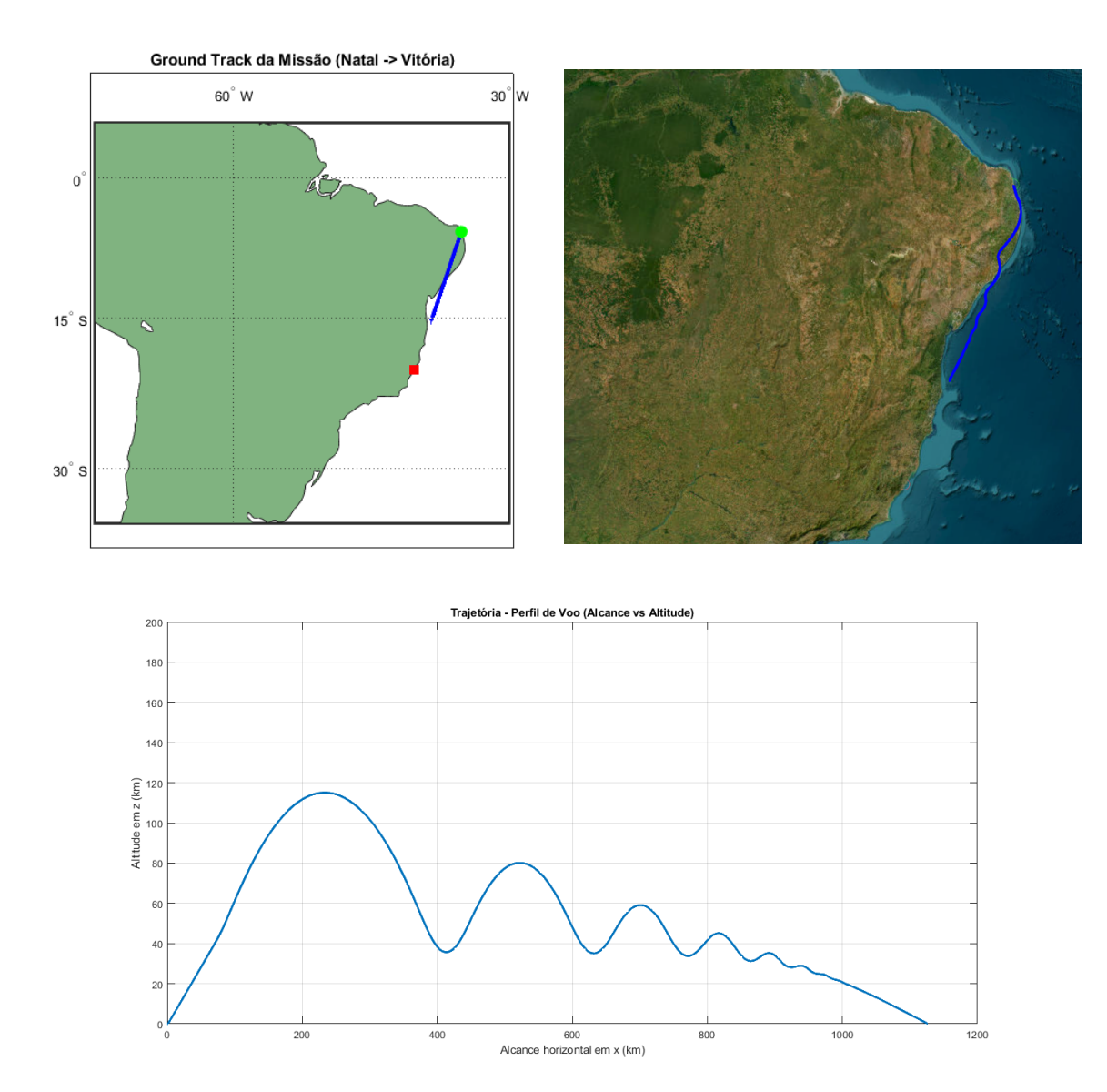


FIGURE 4.1 – Mission Profile. In the upper images, the mission's ground track with a view of Brazil and a three-dimensional top-down view of the trajectory on the globe. Below, the two-dimensional flight profile.

The trajectory demonstrates that the point-mass model, governed by the constructed state-machine model, was able to generate a coherent flight profile. The vehicle executes a steeper ascent, followed by a suborbital ballistic phase and a controlled, and as much as possible, gliding descent towards the target. Throughout this course, the optical sensor would be active, imaging a continuous swath of territory. The total ground distance covered was approximately 1126.74 km, with a total flight time of 2595.85 seconds, and its phases are well evidenced in the graph:

1. Ascent - between 0 and approximately 233 km of range, the vehicle follows a powered ascent trajectory at a fixed angle, followed by a ballistic flight after engine cut-off, reaching the apogee of approximately 115.08 km altitude at 233 km of horizontal

range, after 296.6 seconds.

2. Descent and Reentry - from 233 km altitude [sic], the vehicle begins its descent, but, as can be noted, the trajectory is neither a simple ballistic parabola nor a smooth glide. The graph reveals a series of pronounced "skips" (bounces).

The phenomenon that generates these skips in the atmosphere is called *skip-glide*. When the vehicle dives into the atmosphere, it gains very significant speed. With this, upon entering the region where air density starts to become relevant (approximately below 40 km altitude), combined with the high speed, it generates lift greater than the vehicle's weight, via Equation 3.3. This phenomenon is very common in aerodynamic vehicles with lift greater than that needed just for equilibrium flight.

This damped oscillatory behavior is a direct result of choosing a constant and positive C_L during the hypersonic free-flight phase. In a real vehicle, this trajectory would be actively controlled (GNC), but the physical phenomenon is the same. The presence of this behavior in the simulator is an excellent indicator that the physical model, although simplified, is correctly capturing the interaction between aerodynamic forces and flight dynamics at high speeds.

From a mission perspective, a *skip-glide* trajectory is often desirable, as it allows for significantly increasing the vehicle's horizontal range (permitting the Natal-Vitória transit) and managing thermal loads during reentry, by "skipping" out of the dense atmosphere and allowing the vehicle to radiate heat.

It is interesting to observe how, even taking into account lift and drag throughout the entire trajectory, it closely resembles a free launch in a vacuum above 40 km, reaching an apogee of approximately 115.08 km at 233 km of horizontal range. This result is easily understandable when analyzing the air density, which at this altitude is already on the order of 10^{-3} and continues to decrease to the order of 10^{-7} near 100 km altitude.

In a close-up, it is possible to better observe the flight profile during takeoff.

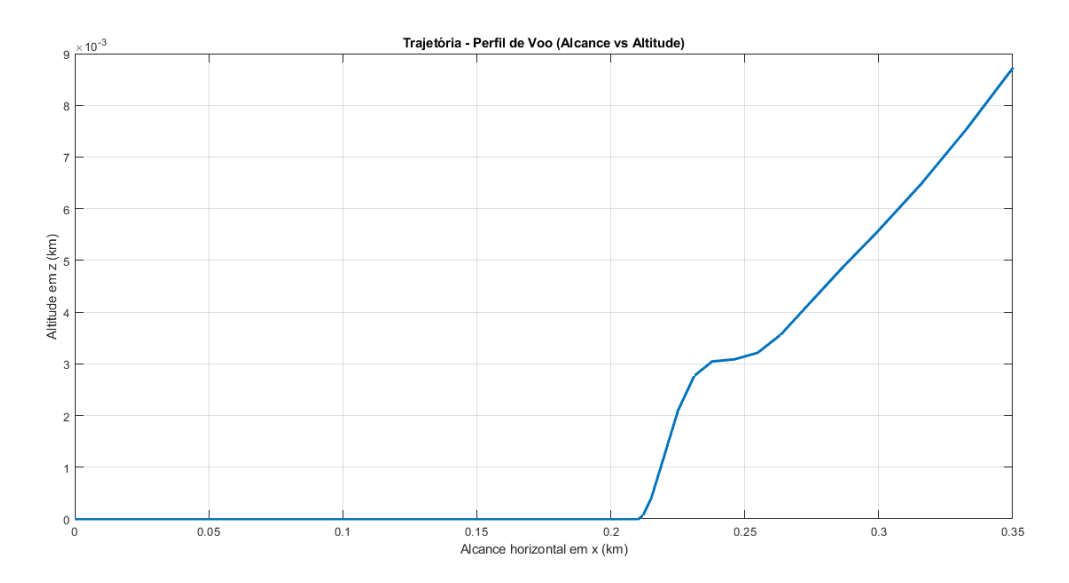


FIGURE 4.2 – Flight profile during takeoff.

As expected, the vehicle follows a horizontal trajectory at zero altitude for approximately 7.65 seconds before the lift force overcomes the vehicle's weight and it effectively takes off. The vehicle's initially abrupt climb, followed by an adjustment that smooths its ascent trajectory, is a result of the simplified model being used. To keep the vehicle on the ground during takeoff, the vertical force (F_z) is forced to be zero. However, as soon as it takes off, the model starts using the vertical force calculated by the 4th Order Point Mass Forces block which, at that instant, is significantly high and, therefore, makes the vehicle climb abruptly. At this moment, the PID controller also kicks in and starts tracking the defined flight path angle $(\gamma_{subida} = 30^{\circ})$, which explains why the vehicle quickly adjusts and begins a reasonable ascent trajectory.

4.2.2 Analysis of flight profiles

For a more detailed analysis of the vehicle's performance, graphs of key simulation parameters were extracted, such as altitude, velocity, and the acting forces.

Velocity profile

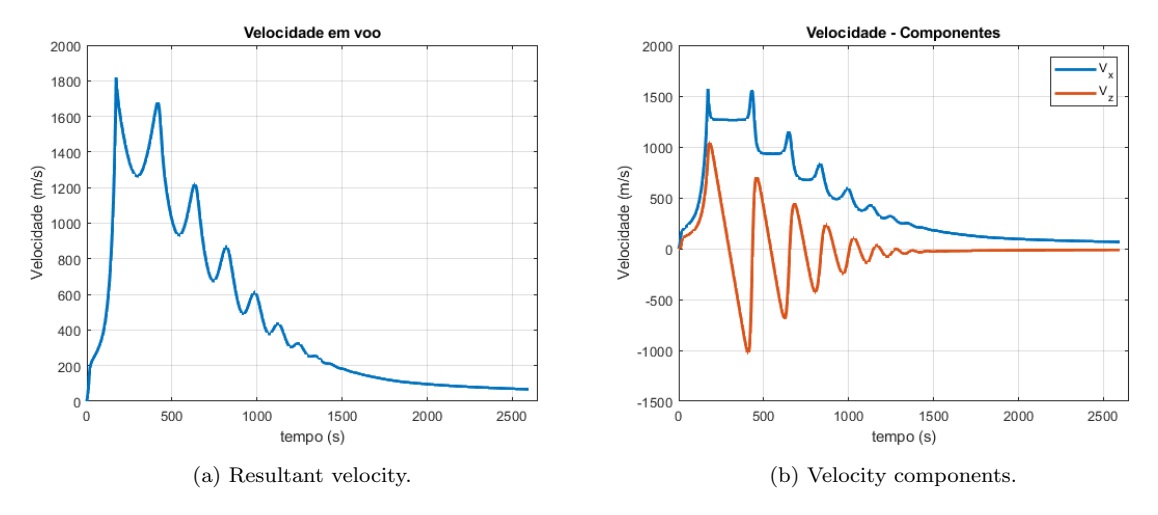


FIGURE 4.3 – Behavior of the aircraft's velocity throughout the flight.

The velocity profile throughout the flight also follows the expected behavior. The sharp increase at the beginning refers to the engine-on phase, a region where the velocity rises to a maximum of approximately 1817.5 m/s (approximately Mach 5.66) after 171.7 seconds. Shortly after, the vehicle loses speed, both due to drag and the fact that it is only under the action of gravity, regaining speed after reaching apogee, when the vehicle begins its descent. From this point, the velocity oscillates to the same extent as the *skip-glides* the vehicle goes through, reaching a lower local maximum velocity with each "skip."

It is important to observe that the maximum velocity reached exceeds Mach 5, thus entering the hypersonic region. As already explained, this is not a very satisfactory result, but it will be overlooked here. This is because, besides the fact that the velocity did not exceed Mach 5 by much, this occurs in a region of much lower air density than at sea level (the vehicle reaches Mach 5 at an altitude of approximately 40.4 km, where the air density is approximately 3.74×10^{-3}). Therefore, the aerodynamic effects of the subsonic regime will be less pronounced, especially considering a simplified and conceptual model like the one proposed here. It is clear that for future stages of the project, it would be necessary to choose between implementing hypersonic regime calculations in the model or adjusting its operation to better fulfill the mission without needing to exceed the speed of 1700 m/s during flight. This will be better discussed later.

Furthermore, an interesting observation is that the vehicle's final velocity was 67.3 m/s (with $V_x \approx 63.27$ m/s and $V_z \approx -11.7$ m/s), which is very consistent with the average speed at which aircraft usually land on runways (between 66.5 m/s and 75 m/s, approximately). The vertical component's velocity would need to be reduced more, in magnitude, for landing, but this would require a specific landing maneuver, which is outside the scope of the present work.

A close-up of the first seconds of flight allows for a better analysis of the velocity profile during takeoff:

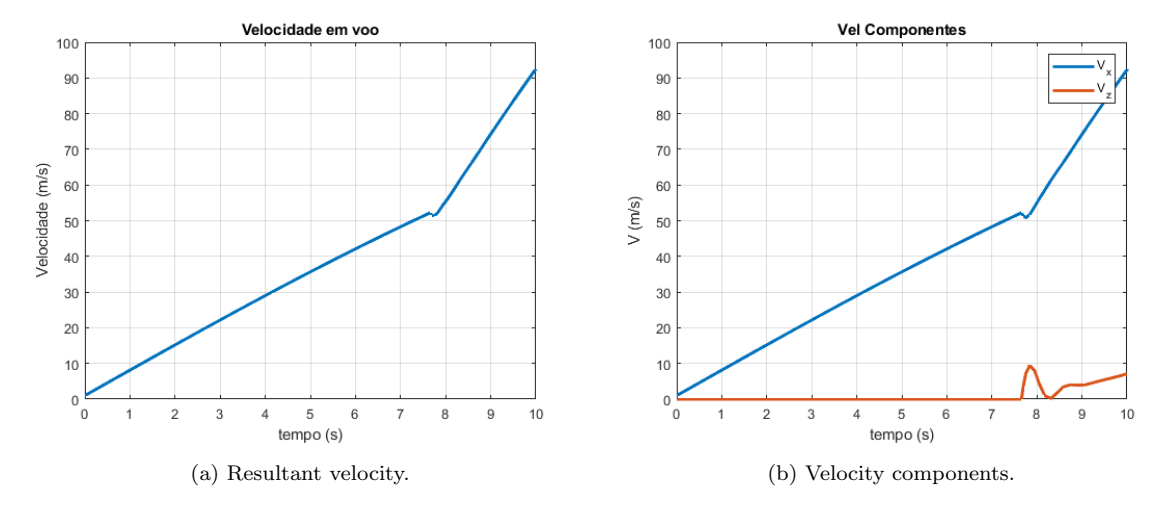


FIGURE 4.4 – Behavior of the aircraft's velocity at takeoff.

As expected, until 7.65 seconds, when takeoff occurs, the velocity in the z-axis is zero and the velocity in the x-axis increases almost linearly, as it is the result of the resultant force (thrust - drag). The thrust is constant and the drag, despite increasing with the increase in velocity, can be considered almost constant acceleration during takeoff, given the low speed and the chosen aerodynamic coefficient parameters. The apparently anomalous behaviors of the velocity components in the few moments following takeoff are due, again, to the abrupt change in vertical force, the C_L , and the action of the PID controller that kicks in at this moment and is tracking the defined flight path angle.

Altitude profile

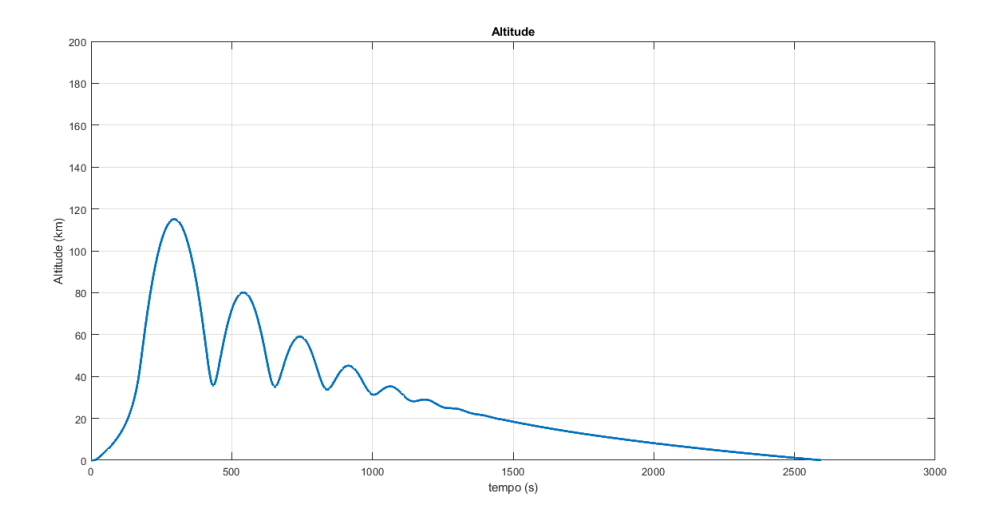


FIGURE 4.5 – Behavior of the aircraft's altitude throughout the flight as a function of time.

The obtained altitude profile is very consistent with all other results obtained so far. The most relevant detail to point out from the graph is how the smooth and controlled descent becomes evident after the *skip-glide* phenomenon ceases to occur. This aligns with what is observed in the graphs of Figure 4.3, as it occurs due to the significant reduction in velocity (and its components) in this phase of the flight, owing to drag in the region of the atmosphere where air density is considerable.

Aerodynamic forces profile

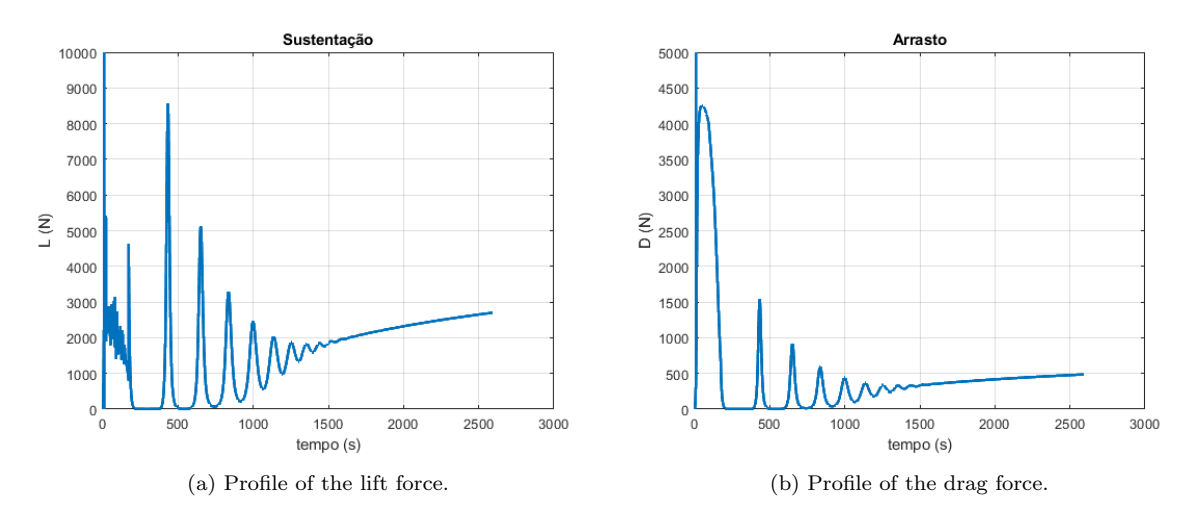


FIGURE 4.6 – Behavior of the aerodynamic forces in the aircraft throughout the flight.

The general behavior of the graphs corresponds to what is expected. Both forces reach considerably high values shortly into the flight, when the vehicle gains significant speed and the atmosphere's density is still high, but drop to practically zero between approximately 200 and 400 seconds, the region where the vehicle is in its ballistic flight in a very rarefied atmosphere. From this point, the forces exhibit an oscillatory character, consistent with the pronounced *skip-glide* phenomenon observed, i.e., the vehicle quickly gains lift and drag during descent, climbs again, and therefore, the value of these forces plummets again, which repeats with decreasing prominence at each skip. Each peak in the force graphs (Figures 4.6a and 4.6b) corresponds to a trough (point of minimum altitude) in the trajectory in Figure 4.1. At the end of the flight, it is possible to identify the behavior of a gradual increase in the value of the forces, a consequence of the fact that, despite the significant reduction in velocity in this region, the increase in air density is contributing more.

However, it is important to address some apparent anomalies in the graphs. Firstly, the graphs presented are cropped for better visualization. Both have a discontinuity that occurs at the transition between the takeoff phase and the powered ascent phase, causing the drag to reach a value of about 12400 N and the lift, a peak of about 27500 N followed

by a negative value of about -600 N, for a very brief instant of time. The lift shows similar behavior at approximately 170 seconds, when the transition from the powered flight phase to free flight occurs. The drag also has a discontinuity at this point, but it is too small to be perceived on the graph's presented scale. This is a consequence of the state machine model being used, which is confirmed by it occurring at its transitions. The abrupt changes in values are a direct result of the *Switch* blocks, which alter the model parameters (like C_L and Thrust) when the state transition conditions are met, and of the PID controller, which has a short tracking period until the flight parameters adjust.

Furthermore, the behavior of the lift during the powered ascent phase might also seem strange: it appears to be noisy, i.e., its value varies rapidly throughout the flight, although the curve follows a trend. This behavior is a result of using the PID controller for this phase. The controller forces the flight path angle to remain constant and, to do so, needs to continuously vary the C_L , given that velocity and air density are varying non-linearly and not directly related throughout the ascent. With C_L , velocity, and air density varying continuously and rapidly, the result is a "confused" lift curve at each point, but with a coherent trend (lift decreases throughout the ascent).

Therefore, the oscillations and discontinuities are not errors, but rather the faithful representation of the dynamics of a point-mass model with parameters controlled by a discrete state machine, subjected to a reentry flight with lift.

4.2.3 Model Limitations and Next Steps

It is fundamental to recognize the simplifications adopted and their limitations, which define the next steps for the evolution of this project. The current model, although functional for a proof of concept, has clear gaps that need to be addressed:

- The point-mass model does not consider the vehicle's attitude dynamics (rotations), which is crucial for sensor pointing and stability. The 2D simulation ignores the need for lateral maneuvers (bank angle) for course correction or to align with the landing runway. Therefore, an evolution to a 6 Degrees of Freedom (6-DOF) Model makes a lot of sense.
- Furthermore, the C_L was kept constant during takeoff and free flight, whereas in a real flight it would be actively modulated by a GNC system to reach a precise target, which should also be implemented via a closed loop. This would further optimize the trajectory and better control the skip-glide phenomenon instead of just observing it.
- Uncertainty Modeling: Add atmospheric perturbations and parameter uncertainties to perform robustness analyses, such as Monte Carlo simulations.

- Complementation of flight profile and range: the case study demonstrated a range limitation (approximately 1123 km simulated versus the 1700 km actual route). The next step is to complement the model, adding new states to the state machine to allow for an engine burn at apogee. This would permit a horizontal cruise flight at high altitude, enabling precise control of the final range. This implementation would also mitigate the problem of entering the hypersonic region, as the vehicle could generate the desired range with a lower and more controlled speed. This modification will require more refined control of mass variation and the implementation of a new controller (like a PID) to manage this flight phase.
- Integration with the Conceptio laboratory's VD (*Virtual Demonstrator*): this integration, to be carried out via MQTT protocol, is an essential next step to validate the model in a broader simulation environment and, mainly, to give it a practical and relevant use.
- Broader feasibility study: since the present work focused on the technical feasibility
 of the simulation. A crucial next step is to conduct an in-depth study on the
 operational, financial, and technological feasibility for Brazil to actually develop a
 real project of a vehicle with these characteristics.

Despite the limitations, the developed simulator fulfills its role as a preliminary analysis tool, providing a solid and validated foundation that captures complex flight dynamics, essential for future iterations.

5 Conclusion

This graduation thesis had as its central objective to investigate the technical feasibility of using a reusable suborbital vehicle, referencing the Dawn Mk-II Aurora, equipped with an optical sensor, the Chameleon, for *on-demand* monitoring missions of the Brazilian territory. The project's motivation lies in the strategic need to overcome the temporal resolution gap of current orbital systems, offering a rapid response capability to dynamic events on the vast national coast and territory.

To answer the research question, a simulation methodology was developed based on a two-dimensional point-mass model, implemented in the *MATLAB/Simulink* environment. The flight logic was structured as a finite-state machine, using blocks from the *Aerospace Blockset* for dynamics propagation and a PID controller for the ascent phase, demonstrating a robust approach for trajectory analysis.

The developed simulator proved successful in its fundamental objectives. It was able to generate a complete mission profile, from takeoff to landing, successfully simulating a suborbital flight. The most significant result of the model was the capture of complex flight dynamics, notably the *skip-glide* phenomenon during atmospheric reentry. The analysis of altitude, velocity, and, especially, aerodynamic force profiles validated the model: the oscillations and discontinuities observed in the lift and drag graphs corresponded perfectly to the state machine transitions and the physics of reentry with lift, attesting to the simulator's fidelity to its theoretical premises.

The Natal-Vitória route case study allowed for a direct answer to the research question. The simulation demonstrated that the suborbital flight concept for this mission is technically feasible. However, the analysis revealed a critical discrepancy between the desired range (about 1700 km) and the obtained range (about 1127 km). This is not a flaw in the simulator, but rather the main discovery of the study: the simple ballistic flight profile, even with *skip-glide*, is insufficient for the proposed mission, and the model requires some implementations before it can move to a possible next development phase.

This result is fundamental, as it clearly defines the next steps for the project. It is concluded that, for the operational feasibility of the concept, it is imperative to evolve the model to include a cruise phase with the engine on at apogee. This high-altitude

propulsion capability would allow for precise control of the horizontal range, solving the identified limitation and, at the same time, mitigating the entry into high-speed hypersonic regimes, which was another observed limitation.

This work, therefore, fulfills its role as a successful proof of concept. It provides a validated simulation tool and a solid foundation upon which future iterations can be built. The recommendations for implementing a 6-DOF model, developing a GNC system, and, crucially, integrating the simulator with the Conceptio laboratory's *Virtual Demonstrator* (VD), establish a clear roadmap for the continuation of the research, contributing to the advancement of national technological maturity in strategic aerospace systems.

Bibliography

Agência Espacial Brasileira. Observação da terra e coleta de dados. Atualizado em 10/10/2023, mar 2020. Available at: https://www.gov.br/aeb/pt-br/acoes-e-programas/aplicacoes-espaciais/observacao-da-terra-e-coleta-de-dados.

Agência Espacial Brasileira. **VSB-30**. 2020. Página atualizada em 17 de outubro de 2023. Available at: https://www.gov.br/aeb/pt-br/acoes-e-programas/aplicacoes-espaciais/transporte-espacial/vsb-30.

Agência Espacial Brasileira. Catálogo da Indústria Espacial Brasileira - 2ª Edição. [S.l.], 2022. Available at: https://www.gov.br/aeb/pt-br/centrais-de-conteudo-/publicacoes/catalogo-da-industria-espacial-brasileira/catalogo-de-fornecedores-do-centro-espacial-de-alcantara/2-edicao-catalogo-da-industria-espacial-brasileira.pdf.

Airport Technology. **Dawn Mk-II Aurora Spaceplane**. 2024. [Accessed 2025-06-10]. Available at:

https://www.airport-technology.com/projects/dawn-mk-ii-aurora-spaceplane/.

ANDERSON, J. D.; EBERHARDT, S. **Introduction to Flight**. 9th. ed. New York, NY: McGraw-Hill Education, 2021. ISBN 978-1260571618.

BELLI, R.; PANESI, F.; VETRISANO, M.; D'ERRICO, M.; GRASSI, M. Physical modeling and simulation of reusable rockets for gnc verification and validation. **Aerospace**, v. 11, n. 5, p. 337, 2024. Available at: https://www.mdpi.com/2226-4310/11/5/337.

BHATT, S. **High-Fidelity Real-Time Trajectory Optimization for Reusable Launch Vehicles**. [S.l.], 2006. Available at: https://apps.dtic.mil/sti/tr/pdf/ADA460473.pdf.

Blue Origin. **New Shepard**. 2024. Available at: https://www.blueorigin.com/new-shepard.

BOCCIA, A.; LELLA, M. D.; FASANO, G.; GRASSI, M.; IACOBELLIS, M.; LANZUISI, S.; MARRA, M.; MONTI, R.; NARDONE, A.; PAPINI, M.; PASCUCCI, C.; PEVERINI, R.; PICCIOTTO, R.; ROMANO, F.; SCOGNAMIGLIO, A.; SPILLER, P.; ZANNINO, E. End-to-end gnc solution for reusable launch vehicles. **MDPI**, v. 12, n. 4, p. 339, accessed:, 2023. Available at: https://www.mdpi.com/2226-4310/12/4/339.

Carlos Alberto Steffen. Introdução ao sensoriamento remoto. s.d. Available at: http://www3.inpe.br/unidades/cep/atividadescep/educasere/apostila-.htmhttp://www3.inpe.br/unidades/cep/atividadescep/educasere/apostila.htm.

BIBLIOGRAPHY 57

CARR, J. Virgin Galactic Space Vehicles Fact Sheet. [S.l.], 2011. Available at: https://www.galacticexperiencesbydeprez.com/pdf/vg_vehicles_fact_sheet101411.pdf.

Copernicus. **S2 Mission**. s.d. Available at:

https://sentiwiki.copernicus.eu/web/s2-mission.

Dawn Aerospace. Dawn mk-ii aurora - rocket-powered aircraft. Accessed 2025-06-10, 2024. Available at: https://www.dawnaerospace.com/spaceplane.

Dragonfly Aerospace. **Chameleon Imager**. 2024. [Accessed 2025-06-10]. Available at: https://dragonflyaerospace.com/products/chameleon/.

EBSCO. Kármán line. Accessed:, 2024. Available at:

https://www.ebsco.com/research-starters/astronomy-and-astrophysics/karman-line.

Empresa Brasileira de Pesquisa Agropecuária (Embrapa). Satélites de monitoramento: Missões landsat. 2020. Available at:

https://www.embrapa.br/satelites-de-monitoramento/missoes/landsat.

FAA. Returning from space. Accessed:, 2007. Available at:

https://www.faa.gov/sites/faa.gov/files/about/office_org/headquarters_offices/avs/III.4-.1.7_Returning_from_Space.pdf.

GIM International. Earth observation sensors and technology: the current state of play. [Accessed 2024-05-15], 2024. Available at: https://www.gim-international.com/content/article/earth-observation-sensors-and-technology-the-current-state-of-play.

GOODELL, M. R.; ELROD, W. C. Suborbital launch trajectories for satellite delivery. **Journal of Spacecraft and Rockets**, v. 32, n. 3, p. 411–416, 1995. Available at: https://doi.org/10.2514/3.26630.

HAYA, R.; ZAIACOMO, G. D.; SERNA, J.; SIPPEL, M.; MOLINA, R. Gnc requirements of for a long range hypersonic transport system. *In*: **18th AIAA/3AF** International Space Planes and Hypersonic Systems and Technologies Conference. **Proceedings** [...]. American Institute of Aeronautics and Astronautics, 2012. Available at: https://elib.dlr.de/78209/1/ISPHST2012 RHaya-FAST20XX final.pdf.

House Committee on Science, Space, and Technology. The emerging commercial suborbital reusable launch vehicle market. Accessed:, Aug 2012. Available at: https://science.house.gov/index.cfm?a=Files.servefile_id=6253997E-D31B-4BB5-B769-797378E53B9.

IDU. Rocket propulsion elements. Accessed:, 2024. Available at: https://ftp.idu.ac.id/wp-content/uploads/ebook/tdg-/DESIGN%20SISTEM%20DAYA%20GERAK/Rocket%20Propulsion%20Elements.pdf.

Instituto Brasileiro de Geografia e Estatística (IBGE). Áreas territoriais - Área de 2024. Publicado no Diário Oficial da União (DOU) Nº 72, de 15 de abril de 2025, conforme Portaria Nº PR-470, de 14 de abril de 2025., 2024. Available at:

https://www.ibge.gov.br/geociencias/organizacao-do-territorio/estrutura-territorial-/15761-areas-dos-municipios.html.

BIBLIOGRAPHY 58

Instituto Nacional de Pesquisas Espaciais. Perguntas frequentes sobre focos de queimadas. 2025. Available at:

https://terrabrasilis.dpi.inpe.br/queimadas/portal/faq/index.html.

INTERNATIONAL ORGANIZATION FOR STANDARDIZATION. **Standard Atmosphere**. 1975. First edition 1975-05-15. Identical with the ICAO and WMO Standard Atmospheres from -2 to 32 km [cite: 5].

Kevin Enright (UP42). **An introduction to optical satellite imagery**. sep 2022. Available at: https://up42.com/blog/introduction-optical-satellite-imagery.

Marinha do Brasil. Novo mapa do brasil é expandido com 5,7 milhões de km² de área marítima. Atualizado em 28 Setembro, 2023, set 2023. Available at: https://www.agencia.marinha.mil.br/amazonia-azul/novo-mapa-do-brasil-e-expandido-com-57-milhoes-de-km²-de-area-maritima.

MIELE, A. **Flight Mechanics: Theory of Flight Paths**. Reading, Massachusetts: Addison-Wesley Publishing Company, Inc., 1962. Originally published as Volume I of the Addison-Wesley Series in the Engineering Sciences. Unabridged republication by Dover Publications, Inc., Mineola, New York, 2016.

NASA. Materials for launch vehicle structures. Accessed:, 2017. Available at: https://ntrs.nasa.gov/api/citations/20170001809/downloads/20170001809.pdf.

NASA. Remote Sensing. s.d. Available at:

https://www.earthdata.nasa.gov/learn/earth-observation-data-basics/remote-sensing.

NASA. **Sentinel-1**. s.d. Available at:

https://www.earthdata.nasa.gov/data/platforms/space-based-platforms/sentinel-1.

NASA Glenn Research Center. Hypersonic flight. Accessed:, 2024. Available at: https://www.grc.nasa.gov/www/BGH/hihyper.html.

NASA Johnson Space Center. Thermal protection systems. 2024.

NASA Wallops Flight Facility. Sub orbital. Accessed:, 2024. Available at: https://go.nasa.gov/WFF_soundingrockets.

SAHINOGLU, M. Modeling and simulation in engineering. Wiley Interdisciplinary Reviews: Computational Statistics, v. 5, n. 3, p. 239–266, 2013.

SARIGUL-KLIJN, M.; SARIGUL-KLIJN, N. Flight mechanics of manned suborbital reusable launch vehicles with recommendations for launch and recovery. **ResearchGate**, accessed:, 2003. Available at: https://www.researchgate.net/publication-/237448317_Flight_Mechanics_of_Manned_SubOrbital_Reusable_Launch_Vehicles_with_Recommendations.

Secretaria do Meio Ambiente (SEMA). Caracterização da zona costeira do brasil. Acessado via Portal do Governo da Bahia, 2007. Available at: https://www.ba.gov.br/meioambiente/137/caracterizacao-da-zona-costeira-do-brasil.

Specim. **Hyperspectral Cameras for Drones - Specim AFX**. 2024. [Accessed 2024-05-15]. Available at: https://www.specim.com/afx/.

BIBLIOGRAPHY 59

WHELAN, M. **X-15 Space Pioneers Now Honored as Astronauts**. June 2013. https://www.nasa.gov/feature/x-15-space-pioneers-now-honored-as-astronauts. Acesso: 8/6/2025.

Wikipedia. Reusable launch vehicle. Accessed:, 2024. Available at: https://en.wikipedia.org/wiki/Reusable_launch_vehicle.

Ximea. xiSpec - Smallest and lightest hyperspectral imaging cameras. 2024. [Accessed 2024-05-15]. Available at: https://www.ximea.com/products/hyperspectral-imaging-/xispec-hyperspectral-miniature-cameras.

Appendix A -

A.1 Script in MATLAB used

```
|%% Par metros do Ve culo Suborbital Simplificado (Dawn Mk-II Aurora)
2 % Script para Trabalho de Gradua
3 % T tulo: Simulador de ve culo suborbital para monitoramento do
     territ rio
4 % brasileiro
5 % Autor: Breno Felipe Penido Morato - Nov/2025
7 clear; clc;
9 % --- Par metros F sicos ---
10 m_inicial = 280.0; % Massa de decolagem (kg)
g = 9.81; % Acelera o da gravidade (m/s^2)
14 % --- Par metros Aerodin micos ---
| \text{rho} = 1.225; % Densidade do ar ao n vel do mar (kg/m^3)
_{16} A = 7.5;
                  % rea da asa (m^2) - Estimativa para comprimento de
    4.8m
17 CLO = 0.1;
                 % Coef de sustenta o m nimo
18 CL_alpha = 2.8; % Coeficiente de Aumento de Sustenta o por radiano
     de AoA
19 CD_min = 0.02; % Coeficiente de arrasto m nimo (AoA zero)
20 k_drag = 0.2;
                 % Fator de arrasto induzido
22 % --- CL's ---
^{23} CL_dec = 0.2;
24 CL_livre = 0.13;
26 % --- Par metros de Propuls o ---
27 T_dec = 2000; % Empuxo de decolagem
T_{voo} = 6000;
                 % Empuxo de subida
30 % --- Par metros da Fase de Voo ---
31 gamma0 = 0; % ngulo de trajet ria inicial
```

```
32 \mid h0 = 0;
               % Altitude inicial
33 \times 0 = 0;
               % Posi o inicial
 VO = 1;
               % Velocidade inicial
35
36 % --- Para Voo Livre ---
 h_meco = 42000; % Altitude de corte do motor (m)
38
39 %% Gera
            o de Dados da Atmosfera Padr o (ISA)
_{41} R = 287.058; % Constante dos gases para o ar seco (J/(kg K))
g0 = 9.80665; % Gravidade as n vel do mar (m/s^2)
43 TO = 288.15; % Temperatura ao n vel do mar (K)
44 PO = 101325; % Press o ao n vel do mar (Pa)
45
_{46} % Defini o das camadas da atmosfera (h em m, L em K/m)
47 h_camadas = [0, 11000, 20000, 32000, 47000, 51000, 71000, 80000];
48 \mid L_{camadas} = [-0.0065, 0, 0.001, 0.0028, 0, -0.0028, -0.002, 0];
49
_{50} h_lookup = linspace(0, 100000, 200);
rho_lookup = zeros(size(h_lookup));
52
T_base = T0;
54 P_base = P0;
55
56 for i = 1:length(h_lookup)
      h = h_lookup(i);
58
      camada = find(h >= h_camadas, 1, 'last');
59
      h_base = h_camadas(camada);
60
      L = L_camadas(camada);
61
62
      T_{camada} = T0;
63
      P_{camada} = P0;
      for j = 2: camada
65
          h_b_prev = h_camadas(j-1);
66
          L_{prev} = L_{camadas(j-1)};
67
           if L_prev == 0
68
               P_{camada} = P_{camada} * exp(-g0*(h_{camadas}(j)-h_b_{prev})/(R*)
69
     T_camada));
          else
               T_{prev} = T_{camada};
71
               T_camada = T_prev + L_prev*(h_camadas(j)-h_b_prev);
72
               P_camada = P_camada * (T_camada/T_prev)^(-g0/(L_prev*R));
           end
74
      end
75
      T_base = T_camada;
76
      P_base = P_camada;
77
```

```
78
      % Temperatura e Press o na altitude h
       if L == 0
80
           T = T_base;
81
           P = P_base * exp(-g0*(h-h_base)/(R*T_base));
       else
83
           T = T_base + L*(h-h_base);
84
           P = P_base * (T/T_base)^(-g0/(L*R));
85
86
       end
87
      rho_lookup(i) = P / (R * T);
88
  end
90
  %% Gera o da Tabela de Varia o de Massa
91
92
  h_{max_sim} = 120000; % m
94
95 h_mass_lookup = [0, h_meco, h_max_sim];
96 m_lookup = [m_inicial, m_final, m_final];
98 %% Sim
  sim("modelo_final.slx")
100
  %% Plots
102
104 figure (1)
plot(Dist_x*1e-3, Dist_z*1e-3, 'LineWidth', 2)
title('Trajet ria - Perfil de Voo (Alcance vs Altitude)')
107 xlabel('Alcance horizontal em x (km)')
ylabel('Altitude em z (km)')
109 ylim([0 200])
110 grid on
111
112 figure (2)
plot(tout, vel_voo, 'LineWidth', 2)
title('Velocidade em voo')
xlabel('tempo (s)')
ylabel('Velocidade (m/s)')
117 grid on
118
119 figure (3)
plot(tout, Dist_z*1e-3, 'LineWidth', 2)
title('Altitude')
122 xlabel('tempo (s)')
123 ylabel('Altitude (km)')
124 ylim([0 200])
```

```
125 grid on
126
127 figure (4)
plot(tout, Vx, 'LineWidth', 2)
129 hold on
plot(tout, Vz, 'LineWidth', 2)
131 hold off
132 title('Vel')
133 title('Vel Componentes')
134 xlabel('tempo (s)')
ylabel('V (m/s)')
136 legend('V_x', 'V_z')
137 grid on
138
139 figure (5)
plot(tout, Lift, 'LineWidth', 2)
141 title ('Sustenta o')
xlabel('tempo (s)')
ylabel('L (N)')
144 grid on
145
146 figure (6)
plot(tout, Drag, 'LineWidth', 2)
148 title ('Arrasto')
149 xlabel('tempo (s)')
ylabel('D (N)')
151 grid on
  %% Plot 3D no Globo Terrestre
153
154
155 % --- Defini o do Corredor de Voo ---
lat_inicio = -5.79; % Latitude de Natal (RN)
lon_inicio = -35.20; % Longitude de Natal (RN)
158 lat_fim = -20.31;
                      % Latitude de Vit ria (ES)
lon_fim = -40.33; % Longitude de Vit ria (ES)
161 % --- Extra o dos Dados da Simula
162 alcance_m = Dist_x; % m
altitude_m = Dist_z; % m
165 % --- C lculo do Caminho Geogr fico ---
166 R_terra = 6371000; % Raio da Terra
167
168 % Calcular o azimute (dire o do voo)
azimute = azimuth(lat_inicio, lon_inicio, lat_fim, lon_fim);
170
171 % Converter o vetor de alcance para dist ncia em graus
```

```
dist_rad = alcance_m / R_terra;
  dist_deg = rad2deg(dist_rad);
174
175 % Calcular os vetores de latitude e longitude para cada ponto da
      trajet ria
176 [lat_trajetoria, lon_trajetoria] = reckon(lat_inicio, lon_inicio,
      dist_deg, azimute);
178 % --- Plotagem no Globo ---
uif = uifigure('Name', 'Plot 3D');
180 g = geoglobe(uif);
  geofig = geoplot3(g, lat_trajetoria, lon_trajetoria, altitude_m, 'b', '
182
      LineWidth', 2.5);
184 hold(g, 'on');
  geoplot3(g, lat_inicio, lon_inicio, 0, 'o', 'Color', 'g', 'MarkerSize',
185
  geoplot3(g, lat_fim, lon_fim, 0, 'o', 'Color', 'r', 'MarkerSize', 10);
  hold(g, 'off');
187
188
189 title ('Trajet ria Suborbital 3D');
191 %% Plot de Perfil de Miss o
  % --- Extra o e Convers o de Dados ---
alcance_km = Dist_x * 1e-3; % km
altitude_km = Dist_z * 1e-3; % km
197 % Coordenadas do Corredor (Natal -> Vit ria)
198 lat_inicio = -5.79;
199 | lon_inicio = -35.20;
200 | lat_fim = -20.31;
  lon_fim = -40.33;
201
202
203 % --- C lculo do Caminho Geogr fico ---
_{204} R_{terra} = 6371000;
205 azimute = azimuth(lat_inicio, lon_inicio, lat_fim, lon_fim);
206 dist_rad = alcance_m / R_terra;
207 dist_deg = rad2deg(dist_rad);
208 [lat_trajetoria, lon_trajetoria] = reckon(lat_inicio, lon_inicio,
      dist_deg, azimute);
210 % --- Cria
                o da Figura com Subplots ---
211 figure (8);
212
213 % --- Plot 1: Mapa do Ground Track ---
```

```
214 latlim = [-35 6]; % Limites de Latitude
215 lonlim = [-75 -30]; % Limites de Longitude
axesm('mercator', 'MapLatLimit', latlim, 'MapLonLimit', lonlim);
     geoshow('landareas.shp', 'FaceColor', [0.5 0.7 0.5]);
218 framem on;
219 gridm on;
220 mlabel on;
221 plabel on;
222
     geoshow(lat_trajetoria, lon_trajetoria, 'DisplayType', 'line', 'Color',
223
             'b', 'LineWidth', 3);
title('Ground Track da Miss o (Natal -> Vit ria)');
     geoshow(lat_inicio, lon_inicio, 'DisplayType', 'point', 'Marker', 'o', '
             MarkerEdgeColor', 'g', 'MarkerFaceColor', 'g', 'MarkerSize', 8);
     geoshow(lat_fim, lon_fim, 'DisplayType', 'point', 'Marker', 's',
            MarkerEdgeColor', 'r', 'MarkerFaceColor', 'r', 'MarkerSize', 8);
227
     %% Plot 3D Geogr fico Abstrato (Sem Mapa)
alcance_m = Dist_x(:); % Alcance em metros
      altitude_m = Dist_z(:); % Altitude em metros
233
234 altitude_km = altitude_m * 1e-3; % Altitude em km
235
     % Coordenadas do Corredor (Natal -> Vit ria)
| 1at_{inicio} = -5.79; | 1on_{inicio} = -35.20; | 1on_{inicio} = -35
     lat_fim = -20.31; lon_fim = -40.33;
238
240 % --- C lculo do Caminho Geogr fico ---
_{241} R_terra = 6371000;
242 azimute = azimuth(lat_inicio, lon_inicio, lat_fim, lon_fim);
243 dist_rad = alcance_m / R_terra;
244 dist_deg = rad2deg(dist_rad);
245 [lat_trajetoria, lon_trajetoria] = reckon(lat_inicio, lon_inicio,
            dist_deg, azimute);
246
247 % --- Cria
                                 o do Gr fico 3D ---
figure('Name', 'Trajet ria 3D (Lon/Lat/Alt)');
plot3(lon_trajetoria, lat_trajetoria, altitude_km, 'r', 'LineWidth', 2);
251 hold on;
plot3(lon_inicio, lat_inicio, 0, 'go', 'MarkerFaceColor', 'g', '
            MarkerSize', 8);
plot3(lon_fim, lat_fim, 0, 'rs', 'MarkerFaceColor', 'r', 'MarkerSize',
            8):
254 hold off;
```

```
title('Trajet ria Suborbital 3D');

xlabel('Longitude (graus)');

ylabel('Latitude (graus)');

zlabel('Altitude (km)');

grid on;

view(3);

axis tight;
```

A.2 Block model in Simulink

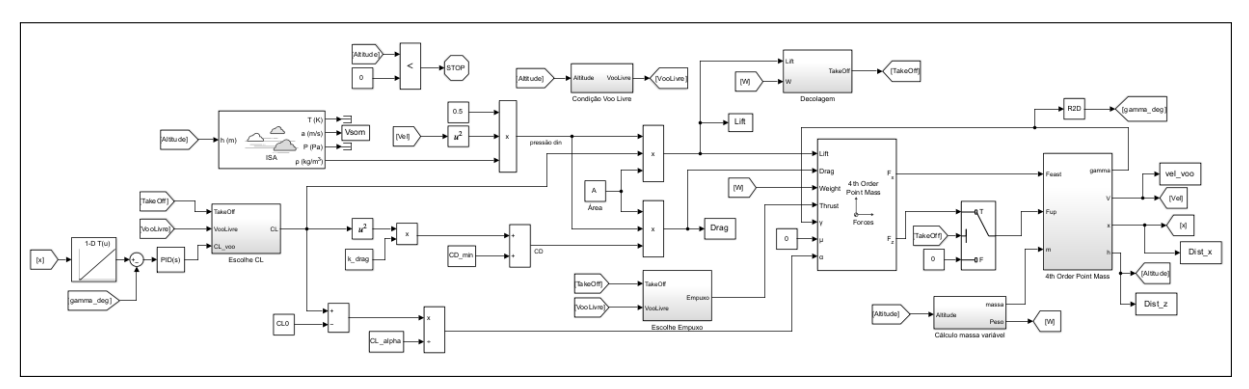
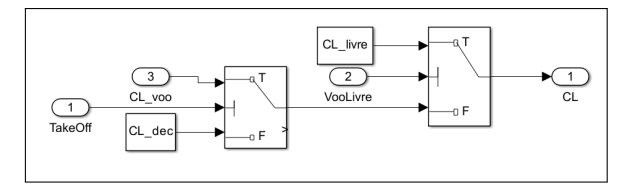
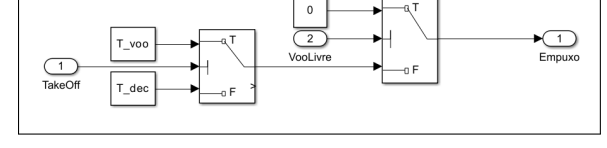


FIGURE A.1 – Complete block model.





- (a) Block "Choose CL" to control what C_L to use in each phase of the flight.
- (b) Block "Choose Thrust" to control how much thrust to use in each phase of the flight.

FIGURE A.2 – Blocks to control the values of C_L and thrust for each phase of the flight.

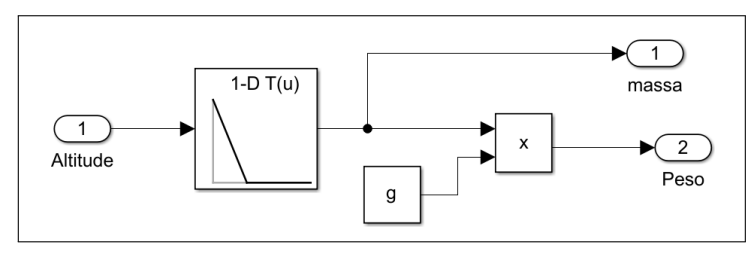


FIGURE A.3 – Block Calculate variable mass to get the variable mass and weight throughout the flight.

FOLHA DE REGISTRO DO DOCUMENTO

1. CLASSIFICAÇÃO/TIPO	^{2.} DATA	^{3.} DOCUMENTO Nº	^{4.} Nº DE PÁGINAS
TC	25 de março de 2015	DCTA/ITA/DM-018/2015	66

Suborbital Vehicle Simulator for Brazilian Territory Monitoring

6. AUTOR(ES):

Breno Felipe Penido Morato

7. INSTITUIÇÃO(ÕES)/ÓRGÃO(S) INTERNO(S)/DIVISÃO(ÕES): Instituto Tecnológico de Aeronáutica – ITA

8. PALAVRAS-CHAVE SUGERIDAS PELO AUTOR:

Suborbital Vehicle; Computational Simulation; Territorial Monitoring; MATLAB/Simulink; Trajectory Analysis; Flight Dynamics

9. PALAVRAS-CHAVE RESULTANTES DE INDEXAÇÃO:

Cupim; Dilema; Construção

¹⁰. APRESENTAÇÃO:

(X) Nacional () Internacional

ITA, São José dos Campos. Curso de Graduação em Engenharia Aeroespacial. Orientador: Cap Av. Lucas Oliveira Barbacovi. Coorientador: Prof. Dr. Christopher Shneider Cerqueira. Defesa em 07/11/2025. Publicada em 21/11/2025.

^{11.} RESUMO:

Este trabalho de graduação propõe o estudo da viabilidade do emprego de um veículo suborbital reutilizável e manobrável para o monitoramento on-demand do território brasileiro, com foco na sua vasta costa. Diante dos desafios das dimensões continentais do Brasil e das limitações temporais de satélites para eventos dinâmicos, veículos suborbitais emergem como solução complementar. O estudo seleciona o veículo Dawn Mk-II Aurora e o sensor óptico Chameleon como bases para a plataforma.

A metodologia centrou-se na construção de um simulador no ambiente MATLAB/Simulink. Foi implementado um modelo de massa-ponto (point-mass) bidimensional, com a lógica de voo estruturada como uma máquina de estados finitos (decolagem, subida motorizada e voo livre). A dinâmica de voo utilizou blocos do Aerospace Blockset e um controlador PID foi aplicado para gerenciar o ângulo de trajetória durante a subida.

Um estudo de caso simulou uma trajetória da costa de Natal (RN) a Vitória (ES). O simulador gerou um perfil de voo completo, atingindo um apogeu de aproximadamente 115 km e um tempo total de voo de 2596 segundos. Notavelmente, o modelo capturou dinâmicas de voo complexas, incluindo o fenômeno de "skip-glide" (quicadas) durante a reentrada atmosférica. A análise dos resultados validou a viabilidade técnica do simulador, porém revelou uma limitação crítica: o alcance horizontal obtido (aprox. 1127 km) foi insuficiente para os 1700 km desejados da rota.

Conclui-se que, para a viabilidade operacional da missão, o modelo necessita de evolução para incluir uma fase de cruzeiro motorizado no apogeu, permitindo o controle preciso do alcance. O trabalho contribui com uma ferramenta de simulação validada e estabelece os próximos passos para a integração com o laboratório ConceptIO.

^{12.} GRAU DE SIGILO:			
(X) OSTENSIVO	() RESERVADO	() SECRETO	

^{5.} TÍTULO E SUBTÍTULO: